Deep Learning for Remote Sensing-Based Estimation of Water Quality Parameters

by

Dinesh Neupane

A thesis submitted to the Graduate Faculty of
Auburn University
in partial fulfillment of the
requirements for the Degree of
Master of Science in Geography

Auburn, Alabama
August 3, 2024

Approved by

Dr. Stephanie Rogers, Chair, Assistant Professor, Department of Geosciences
Dr. Lana Narine, Assistant Professor, College of Forestry, Wildlife and Environment
Dr. Jingyi Zheng, Assistant Professor, Department of Mathematics and Statistic

Abstract

Monitoring and assessing the characteristics of surface water is critical for managing and improving its quality. While the existing *in situ* measurement methods are precise, they have limitations in terms of spatial and temporal coverage and high acquisition costs. Remote sensing data, specifically satellite imagery, has the potential to provide an invaluable complementary source of information at multiple scales of analysis. Incorporating *in situ* measurements with satellite imagery provides a way to estimate water quality parameters at broader scales and with greater temporal frequency. The knowledge gap lies in effectively integrating *in situ* measurements with satellite imagery using deep learning for accurate water quality assessments. Closing this knowledge gap, the application of deep learning, demonstrated efficacy in diverse domains, shows potential for enhancing the water quality parameter estimation process. Although multiple regression techniques and machine learning methods were studied previously to predict water quality parameters, a high-performance deep learning technique that learns higher order statistical relationships between surface reflectance values and water quality parameters is still lacking, and thus, needed. This research proposes a new and cost-effective technique coupling Sentinel-2 imagery and Deep Neural Network (DNN), a deep learning technique to estimate two water quality parameters: Chlorophyll-a and turbidity. The study was focused on Lake Okeechobee, Florida's largest freshwater lake. Surface reflectance values from Sentinel-2 image bands (5304 band images for Chl-a and 5772 band images for turbidity) combined with auxiliary band variables were used to predict the water quality parameters based on *in situ* datasets. A total of 25 feature variables were used for Chl-a and 19 feature variables were used for turbidity. We adopted a common partition ratio of 70/30 for training and testing purposes. We evaluated two machine learning models: Support Vector Regression (SVR), Random Forest (RF), and one DNN model. The proposed exponentially decreasing DNN approach produced results with significantly higher R^2 values, and lower MSE, RMSE, MRE, and MAE values. When applied to the test dataset, the DNN approach showed the highest correlation (R^2=0.62, MSE=0.14, RMSE=0.38, MRE=12.15%, MAE=0.30) for Chl-a and for turbidity (R^2=0.72, MSE=0.14, RMSE=0.37, MRE=9.60%, MAE=0.28). For the Chl-a parameter, the DNN approach outperformed the RF model by 12.7% and the SVR model by 16.9%, when assessed using R^2. Similarly, for the turbidity parameter the DNN approach outperformed the RF model by 18.03% and the SVR model by 28.5% when assessed using R^2. The weights of the trained DNN model can be adapted and fine-tuned for other inland lakes and can be tested on other research areas in the future.

Acknowledgments

I would like to express my sincere gratitude to those who have contributed to the completion of this thesis. Firstly, I extend my heartfelt appreciation to my committee members, Drs. Stephanie Rogers, Jingyi Zheng, and Lana Narine, for their invaluable guidance, insightful feedback, and unwavering support throughout the research process. Their expertise and encouragement have been instrumental in shaping this work.

I am also deeply grateful to the members of the GeoIDEA lab for their suggestions and discussions about the topic. Lastly, I extend my thanks to all individuals, mentors, friends, and family members who have provided encouragement, assistance, and understanding during this journey. Your support has been a constant source of motivation and inspiration.

Thank you all for your invaluable contributions.

Table of Contents

List of Tables

List of Figures

List of Abbreviations

ADAM	Adaptive Moment Estimation
Chl-a	Chlorophyll-a
DNN	Deep Neural Network
GEE	Google Earth Engine
MSI	MultiSpectral Instrument
NDVI	Normalized Difference Vegetation Index
NDCI	Normalized Difference Chlorophyll Index
NDTI	Normalized Difference Turbidity Index
NH3-N	Ammonia-Nitrogen
NTU	Nephelometric Turbidity Unit
OLCI	Ocean and Land Colour Instrument
RF	Random Forest
S2A	Sentinel 2 A
SVR	Support Vector Regression
SFWMD	South Florida Water Management District
TN	Total Nitrogen

1. Introduction

Water quality parameter assessment plays a crucial role in ensuring sustainability and health of our aquatic ecosystems. Different physical instruments like multi-parameter probes, Secchi disks, colorimeters, fluorometers and spectrophotometers are used to measure physical and chemical properties of water in inland lakes and rivers. These instruments are used for on-site measurements of water quality and often require subsequent laboratory analysis for precise quantification of water quality parameters (Wetzel & Likens, 2000). These traditional water quality monitoring techniques, although highly accurate, are vastly insufficient in terms of spatial and temporal coverage (Peterson et al., 2020).

Remote sensing has become an increasingly important tool in water quality analysis, offering several advantages over traditional *in situ* measurements (Gholizadeh et al., 2016). Remote sensing based estimation of water quality involves using satellite imagery to measure the reflectance of light from water surfaces to determine specific water quality parameters (Ritchie et al., 2003a). In recent years, there has been a shift from direct sampling towards using *in situ* data as a validation tool for remote sensing-based monitoring rather than solely relying on it for operational decision-making (Chawira et al., 2013). Satellite-based remote sensing techniques provide an efficient way to monitor waterbodies at coarse spatial and temporal scales (e.g., monitoring water quality of large lakes or rivers at the regional scale over a period of multiple years or seasons) (Ritchie et al., 2003b).

The Earth receives energy from the sun in the form of electromagnetic radiation. This radiation is reflected, absorbed, and emitted by the Earth's surface or atmosphere Figure 1. Satellites carry instruments or sensors that measure electromagnetic radiation reflected or emitted from both terrestrial and atmospheric sources. Different materials reflect and absorb different wavelengths of electromagnetic radiation (Aggarwal, 2004). By analyzing the wavelengths that have been reflected and detected by a sensor, the type of material it reflected from can be determined. This is commonly known as the spectral signature of that material.

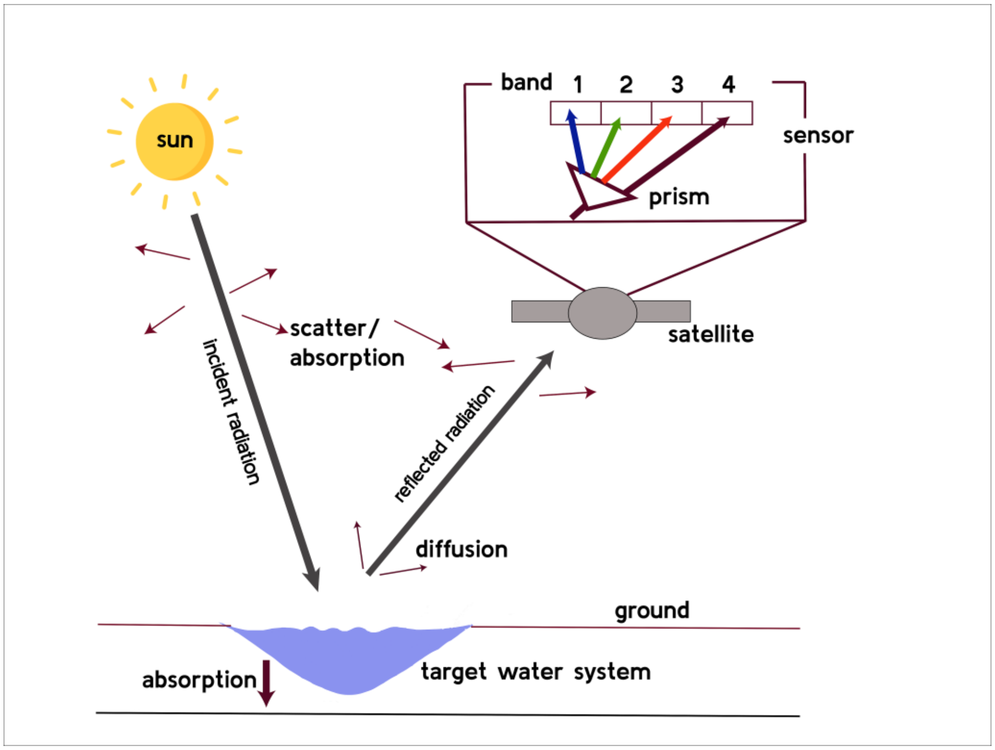

Figure 1 Remote sensing of water- illustration of satellite detection of incident and reflected radiation across different bands in an inland water system

Current satellite missions for water quality monitoring, including Landsat 8, Aqua Moderate Resolution Imaging Spectroradiometer (MODIS), Joint polar Satellite System - Visible Infrared Imaging Radiometer Suite (JPSS VIIRS), Sentinel-2 Multispectral Imaging, and Sentinel-3 Ocean and Land Color Instrument (Sentinel-3 OLCI), operate in polar orbits with varying swath widths and revisit times (Pahlevan et al., 2022). As will be later discussed, previous research has demonstrated the utilization of Sentinel-2 images to estimate various water quality parameters, including both optically active and inactive parameters, based on different band combinations (Guo et al., 2021; Katlane et al., 2020).

Recent advancements in remote sensing technology combined with the power of deep learning has opened new avenues for more efficient and accurate analysis of the water quality parameters (Chebud et al., 2012). Deep learning, a subset of machine learning, has gained significant attention and promising applications in the field of water quality measurement (Ahmed et al., 2022). This approach involves the utilization of artificial neural networks comprising multiple hidden layers to identify complex patterns and produce precise predictions from extensive datasets (Chebud et al., 2012; Peterson et al., 2020). Surface reflectance has been widely used in remote sensing based estimation of water quality parameters and is a reliable water quality estimator for inland lakes and rivers (Ritchie et al., 2003b; Vinciková et al., 2015). Surface reflectance measures the fraction of incoming light reflected off a surface, used to analyze and monitor water quality by identifying substances like chlorophyll and sediments through their light patterns (Vinciková et al., 2015). This research aims to establish a dependable and efficient methodology for the monitoring and evaluation of optically active water quality parameters, such as chlorophyll-a (Chl-a) concentration and turbidity, by training a deep learning model using *in situ* measurements and surface reflectance values derived from corresponding satellite imagery. The study is focused on an inland water system within Florida, specifically targeting Lake Okeechobee. Additionally, we aim to evaluate the efficacy of classical machine learning techniques, specifically support vector regression and ensemble methods like random forest, for predicting water quality parameters.

Early development of remote sensing techniques for water quality measurements began in 1970s which included the measurement of spectral and thermal differences from water surfaces (Ritchie et al., 2003b). Nowadays, remote sensing of water quality involves high resolution multispectral sensors, advanced algorithms and machine learning techniques to analyze data from satellite platforms for continuous monitoring and accurate assessment of water quality parameters (Yang et al., 2022). Recent advancements in remote sensing analytics have significantly improved the ability to extract valuable information from satellite imagery. Key developments include the integration of artificial intelligence and machine learning for improved image processing and classification, leading to more accurate and efficient analysis of large imagery datasets (Chen et al., 2019). Given the recent advances in remote sensing analytics and integration of machine learning infrastructures, it is crucial to evaluate capabilities of remote sensing for water quality monitoring in the context of water resources management and decision-making (Sagan et al., 2020).

Conventional regression models might not be optimal when there a complex, nonlinear relationship between water systems and environmental factors (Claverie et al., 2018). Although multiple machine learning models have been tested in past studies to establish a relationship between satellite data and *in situ* samples, most of them have shown low accuracy in terms of correlation between actual and predicted values. Deep learning techniques provide an opportunity to learn the more sophisticated statistical characteristics between surface reflectance values and *in situ* samples of water quality (Claverie et al., 2018).

2. Research Questions and Hypotheses

This study is designed to understand the potential of deep learning models to retrieve water quality parameters using satellite imagery and *in situ* observations in inland water systems. To guide this research, the following research questions and hypotheses were established:

Research Question 1: Can deep learning models retrieve map water quality parameters from satellite imagery and *in situ* data effectively?

Hypothesis: Deep learning techniques applied to Sentinel-2 imagery can provide accurate and reliable estimates of water quality parameters, such as Chl-a concentration and turbidity, in inland water systems.

Research Question 2: How do deep learning methods compare to traditional machine learning for water quality estimation?

Hypothesis: Deep learning techniques model complex relationships between water quality parameters and surface reflectance values by learning higher order statistical relationships and thus outperform traditional machine learning techniques.

3. Geographical Setting

The study was centered in the state of Florida, USA, known for its diverse geographical features characterized by abundance of inland aquatic systems, like lakes and rivers. The primary focus was on Lake Okeechobee, Florida as shown in Figure 2. which has spatial extent of 1,900 km^2. Lake Okeechobee, Florida's largest freshwater lake, holds a vital position in the region's hydrological system with numerous canals and streams connected to the lake and is primarily used for water supply and flood control (Jin et al., 2000). The South Florida Water Management District (SFWMD) has monitored the inflows to Lake Okeechobee at the District operated control structures and maintained an extensive water quality monitoring network in the Lake Okeechobee watershed since 1972 (J. Zhang et al., 2011). Nutrients (dissolved and suspended) enter the lake via different pathways, including surface water runoff from the surrounding watersheds, atmospheric deposition, and internal nutrient releases (i.e., decomposing plant material and sediment resuspension) (Faridmarandi et al., 2021). Land use and management practices within the watershed directly influence the nutrient levels in surface water runoff (Canfield & Hoyer, 1988; Ha et al., 2021).

The study area has wet and dry seasons as two major climatic seasons (Hajigholizadeh et al., 2021). The wet season spans from June through October, when 70 percent of the year's rain falls, and most hurricanes occur; and the dry season spans from November through May.

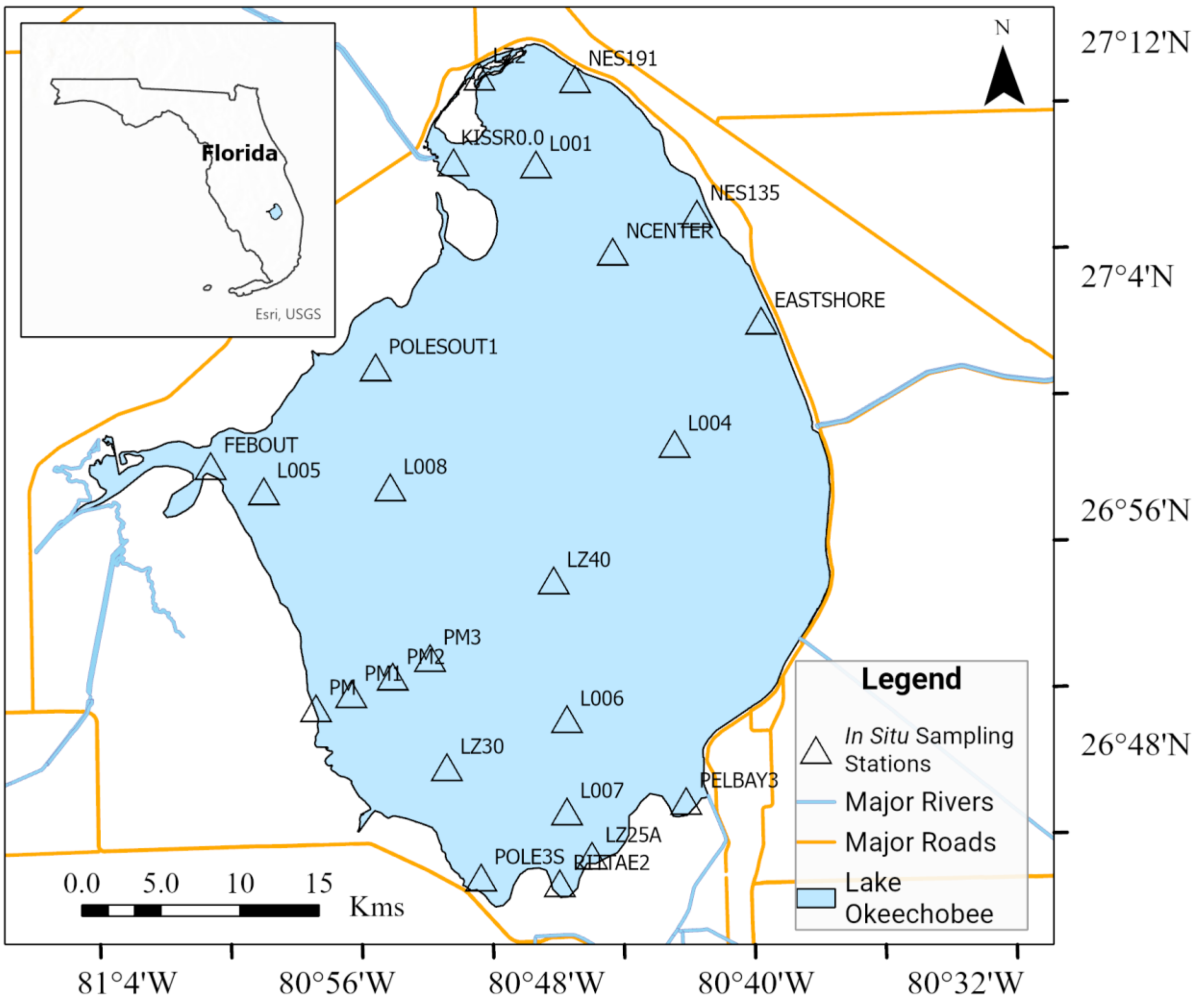

Figure 2. Study area - Lake Okeechobee and in situ measurement stations two water quality parameters spread across the lake

4. Background

4.1. Remote Sensing of Water Quality

Major factors affecting water quality in inland water bodies are suspended sediments (turbidity), algae (i.e., chlorophylls, carotenoids), chemicals (i.e., nutrients, pesticides, metals), dissolved organic matter (DOM), aquatic vascular plants, pathogens, and oils (Ritchie et al., 2003a). These materials are optically active, and they change the energy spectra of reflected solar and/or emitting thermal radiation from surface waters which can be quantified using remote sensing techniques (Gholizadeh et al., 2016; Ritchie et al., 2003b).

Although there are multiple characteristics of water quality, only a few of them like Chl-a, total suspended solids (TSS), and turbidity are optically active meaning they can be detected and measured using optical methods. Their true concentrations cannot be directly measured from remote sensing imagery alone. Preprocessing the data, calibrating with *in situ* measurements, applying appropriate algorithms, and accounting for environmental factors are necessary to estimate accurate concentrations. These steps ensure the derived concentrations closely approximate the true values (Dekker et al., 2002). Their concentrations can be determined by measuring the scattering and absorption of light within the water as proxy. Variables like pH, total nitrogen (TN), ammonia nitrogen (NH3-N) and dissolved oxygen have low signal to noise ratio when measured optically, i.e., their concentrations do not significantly affect the optical properties of water in a way to be easily detectable by sensing instrument. The optical methods for detecting and quantifying these variables may be less precise or more susceptible to interference from other factors. For instance, pH, which is a measure of acidity or alkalinity of water, is best determined using electrochemical methods rather than optical techniques. This study is focused on estimating two important water quality parameters: Chl-a concentration and turbidity of the inland water systems outlined in study area using surface reflectance values as proxy. Surface reflectance is the fraction of light that is reflected by a surface. It is defined as the ratio of the reflected radiance to the incident irradiance. Changes in the concentration of water quality parameters can be detected by measuring changes in surface reflectance values. Surface reflectance measurements are effective for detecting changes in water quality parameters, but their accuracy in providing exact concentrations can vary due to factors like water depth, composition, and atmospheric conditions. Studies have shown that while remote sensing can reliably estimate concentrations of parameters like Chl-a and turbidity, *in situ* calibration and validation are crucial for improving accuracy (Gholizadeh et al., 2016; Kutser, 2009).

4.1.1. Chlorophyll-a (Chl-a)

Chlorophyll-a, often abbreviated as Chl-a, is a pigment found in the chloroplasts of photosynthetic organisms, including algae and plants (Zheng & DiGiacomo, 2017). It is usually measured in micrograms per liter (µg/L). It plays a fundamental role in photosynthesis, capturing sunlight and converting it into chemical energy (Zheng & DiGiacomo, 2017). Algal blooms, which are often driven by eutrophication phenomena in freshwater, are directly related to Chl-a concentration since it is essential for photosynthesis (Lim & Choi, 2015). However, it is important to note that Chl-b, another chlorophyll pigment, complements Chl-a in the photosynthetic process by capturing additional wavelengths of light (Lichtenthaler et al., 1981) (Figure 3). Both pigments are the indicators of abundance and health of phytoplankton and algae in aquatic ecosystems. Elevated levels of Chl-a can signify excessive algal growth, potentially indicating nutrient pollution and poor water quality. Chl-a is the major indicator of overall nutrient status because it acts as a link between nutrient concentration, particularly phosphorus, and algal production (Ouma et al., 2020).

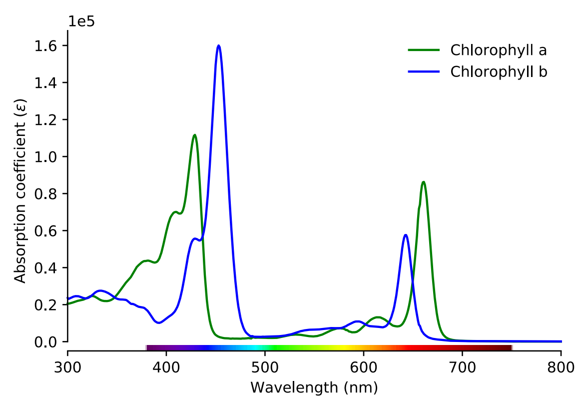

Figure 3. Absorption spectrum of Chlorophyll-a and Chlorophyll-b - absorption coefficients over a range of wavelengths. Absorption coefficients can be empirically converted into reflectance

Chl-a, while mainly reflecting green, absorbs most energy from wavelengths of violet-blue (400-500 nm) and orange-red light (600-700 nm), whose reflectance causes chlorophyll to appear green and the addition of Chl-b along with Chl-a extends the spectrum absorption (Gholizadeh et al., 2016). Chl-a and Chl-b concentrations are measured using satellite remote sensing by utilizing the distinct reflectance patterns in the visible spectrum, particularly around the blue, red and near infrared wavelengths where these pigments absorb light (Dall'Olmo et al., 2005). Chl-a concentrations can be estimated from the reflectance values in the blue (400-500 nm), red (600-700 nm), and near-infrared (NIR) (700-900 nm) bands (Dall'Olmo et al., 2005; Gholizadeh et al., 2016). In addition, combinations of different bands within this wavelength region are used to monitor the concentration of Chl-a as outlined in Table 2.

4.1.2. Turbidity

Turbidity represents the level of suspended sediments in water, indicating water clarity (Garg et al., 2020). It is mainly caused by the presence of silt or algae in a water body, or industrial waste disposed in rivers by mining activity, industrial operations and logging (Garg et al., 2020). Turbidity is usually measured in Nephelometric Turbidity Units (NTU). Turbidity is an important optical property of water, where suspended sediments scatter the light rather than transmit it along the water column (Sebastiá-Frasquet et al., 2019). Turbidity increases as suspended solids or sediment concentration in water increases, leading to increased water opacity, which negatively impacts aquatic life (Garg et al., 2020; Ritchie et al., 2003b). Remote sensing is used to map and monitor this characteristic of water by observing how changes in suspended sediment concentration alter the optical properties of water columns. Existing literature has documented that the surface reflectance, particularly in the red region of the visible spectrum, increases as sediment levels or turbidity rise and reflectance peak shifts from green to red region of the spectrum (Garg et al., 2020; Gholizadeh et al., 2016; Ritchie et al., 1976). Hence, the reflectance in the red and green bands of the visible spectrum is often employed to estimate turbidity. In addition, combinations of different bands within this wavelength region are used to monitor the concentration of turbidity as outlined in Table 2.

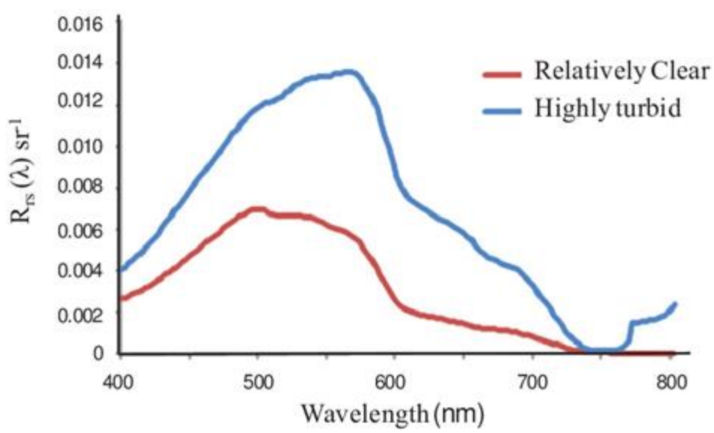

Figure 4. Reflectance spectrum of turbidity – behavior of reflectance values in relatively clear and highly turbid water across various wavelengths

4.2. **Improving Water Quality Estimation Methods**

Multiple studies have used linear regression and machine learning approaches like Logistic Regression, SVR and ensemble methods for water quality parameters estimation (Guo et al., 2021; Muharemi et al., 2019; Sagan et al., 2020). While these methods can provide valuable insights of water quality, they may have limitations when it comes to capturing complex, non-linear relationships in the data. Research by Guo et al., (2021) has highlighted some of these challenges, particularly in the context of water quality parameter estimation using machine learning techniques. They found that while linear regression and SVR models could provide reasonable estimations for certain parameters, they were less effective at capturing non-linear relationships and subtle variations in the data. This study introduced a method to determine the optimal band composition for retrieving different water quality parameters by analyzing 255 band combinations. They also discussed the water quality classification techniques based on the predicted water quality parameters. Additionally, Sagan et al. (2020) have also discussed similar limitations in their studies, emphasizing the need for more sophisticated modeling approaches to overcome these challenges. Akbar et al. (2014) highlighted the development multiple empirical models for modeling Water Quality Index (WQI) based on satellite bands and band combinations to establish relationships between satellite reflectance and water quality variables. The developed empirical equations are specific to individual locations and the study period. Their transferability to other locations may be limited due to variations in water quality parameters, hydrological conditions, and land cover. Machine Learning (ML) is a branch of artificial intelligence where algorithms learn from and make predictions or decisions based on data without being explicitly programmed (Mitchell, 2013). Deep Learning (DL) is a subset of machine learning that uses multi-layered neural networks to automatically learn hierarchical feature representations from the data (LeCun et al., 2015). Deep learning is a powerful technique in machine learning that excels at learning intricate patterns and relationships from data. This enables the model to capture higher order statistical relationships that may be difficult for traditional statistical and machine learning approaches to learn. These models can adapt to a wide range of data distributions and exhibit high flexibility in modeling complex relationships potentially providing more accurate estimations even in situations where traditional approaches struggle. A study by Qian et al. (2022) found that Deep Learning models outperformed classical machine learning techniques like Multiple Linear Regression (MLR), Random Forest (RF) and Support Vector Regression (SVR) in predicting water quality parameters like pH and Dissolved Oxygen (DO). DNN showed a more robust performance

(R^2 =0.89 for pH, R^2 =0.77 for DO) as compared to other machine learning techniques like MLR (R^2 =0.55 for pH, R^2 =0.22 for DO), SVR (R^2 =0.74 for pH, R^2 =0.24 for DO) and RF (R^2 =0.73 for pH, R^2 =0.57 for DO).

4.3. Mapping of Water Quality Parameters using Remote Sensing

In previous studies, the mapping of lake water quality parameters were conducted using Sentinel-2 satellite imagery combined with in situ data using just the band ratios (Toming et al., 2016, 2017). Algorithms utilizing band ratios, such as the height of the 705 nm peak for chlorophyll a (Chl a) and green to red band ratios for colored dissolved organic matter (CDOM), dissolved organic carbon (DOC), and water color, were applied (Toming et al., 2016). In other studies, several types of models, such as stochastic, optimization, dynamic simulation, and empirical statistical models, were employed to predict water quality parameters. These models use a combination of quantitative and qualitative predictors to estimate the outcomes of categorical variables. Subsequently, the predicted water quality parameters were mapped to provide spatial representations (El Ouali et al., 2021). Similarly, Water Quality Index (WQI), which is a composite score that simplifies the assessment of water quality by combining multiple parameters into a single, easy-to-understand value that reflects the overall status of a water body, is also used with Geographic Information System (GIS) tools and clustering techniques to map water quality parameters (Gupta et al., 2015). Spatial interpolation techniques like Krigging and Inverse Distance Weighting (IDW) techniques are also widely used to map water quality variables (Murphy et al., 2010; W. Yang et al., 2020). These methods rely heavily on physical sampling and lab analysis to assess water quality at specific locations. Recently there has been some developments in water quality mapping using machine learning techniques (Adusei et al., 2021) but there is a significant lack of high accuracy mapping techniques. Mapping accuracy of water quality parameters can be significantly improved using deep learning-based regressors that use both spectral bands and their combinations. The model weights and biases can be applied to a combination of spectral bands and band ratios using the deep learning model generated regressor to quantify the water quality parameters across the spatial extent of the images (Ahmed et al., 2022; Rodríguez-López et al., 2023). The advantage of this approach over traditional modeling approach is automatic extraction and learning of relevant features from high-dimensional image data, leading to more precise predictions. This overcomes the drawbacks of traditional models like linear assumptions and manual feature extraction (Ahmed et al., 2022).

4.4. *In situ* Samples

In situ samples of water quality measurements refer to the data collected directly from the water body at the location of interest (Kumar et al., 2024). *In situ* samples play a critical role in water quality remote sensing as they are fundamental for the calibration and validation of the remote sensing models. Collection of *in situ* samples should be at the same time and location as satellite imagery is acquired. The *in situ* data are then used to develop statistical relationships between the water quality parameters and remote sensing reflectance data (Peterson et al., 2020). In the calibration phase, *in situ* measurements serve as the foundation for training algorithms and developing transfer functions that establish mathematical relationships between remote sensing observations (such as reflectance values) and actual water quality measurements (Ahmed et al., 2022).

A study led by Tian et al., (2022) used multiple machine learning algorithms to study the correlation between water quality parameters, including Chl-a, in an inland water system. They collected *in situ* samples directly from the study area, providing precise Chl-a concentrations. A significant correlation of $R^2 > 0.4$ was found between the predicted and *in situ* measurements using all learning models. It was found that different Machine learning models e.g., Extreme Gradient Boosting (XGBoost), Support Vector Regression (SVR) and Random Forest (RF) reflect the intricate and non-linear relationship between water quality parameters and spectral reflectance meaning if the reflectance of the study area does not fluctuate significantly, the values of the water quality parameters, especially Chl-a, in the area do not vary significantly either (Tian et al., 2022). While the study led by Tian et al. (2022) demonstrated a significant correlation between predicted and *in situ* measurements, they acknowledged room for improvement in precision. This acknowledgment likely stems from various factors such as the complexity of the models, the quality and quantity of the input data, the selection and engineering of features, evaluation metrics employed, and the generalization and robustness of the models. The adoption of more sophisticated deep learning models holds promise for refining the estimation process and achieving higher levels of accuracy.

5. Materials and Methods

5.1. Research Method and Design

The overall research method is summarized in the conceptual framework in Figure 5. The conceptual framework outlines a data-driven approach for predicting water quality variables and generating water quality maps using satellite data and machine learning. By leveraging GEE for data access and cloud computing, the method offers a scalable and automated solution for water quality monitoring. First, satellite data from Sentinel-2 is matched with ground truth water quality measurements collected at specific times. Next, features like spectral indices are derived from satellite data. Machine learning models were then trained on these features and the water quality measurements. Finally, the best performing model was used to predict water quality values for new satellite images and to create maps.

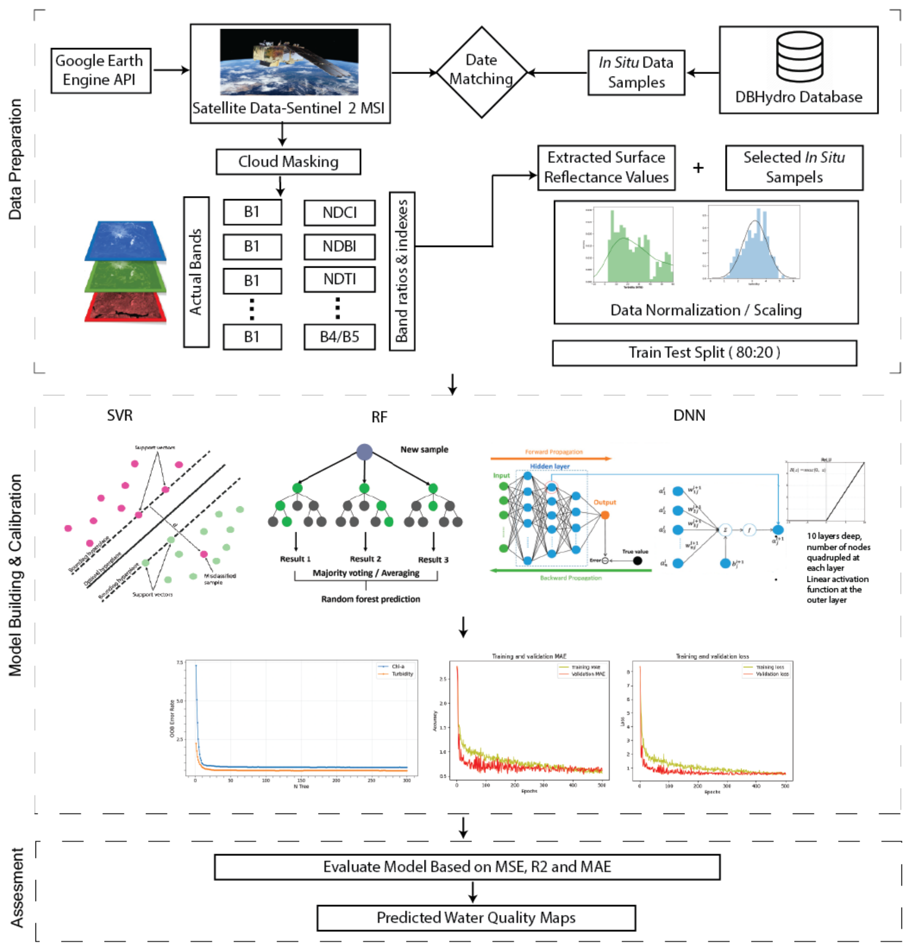

Figure 5. Conceptual framework of methodology showing steps of data collection, preprocessing, model-building, model evaluation and map generation

5.2. *In Situ* Data

In situ data for the measurement of water quality parameters were obtained from South Florida Water Management District's DBHydro (https://www.sfwmd.gov/science-data/dbhydro) platform. DBHydro is the South Florida Water Management District's corporate environmental database that stores hydrologic, meteorologic, hydrogeologic and water quality data. This database is the source of historical and up-to-date environmental data for the 16-county region covered by the District (SFWMD, n.d.). Chl-a and turbidity samples from dates 2015 to 2023 were extracted from DBHydro using dnhydroR, an R interface to the DBHydro Database. Water quality samples from a total of 25 stations as shown in Figure 2 were taken with their corresponding dates.

5.3. Satellite Remote Sensing Data

Sentinel-2 is an Earth observation satellite designed to systematically deliver optical imagery at high spatial resolution (10, 20, and 60 m) over land and waters (Drusch et al., 2012, Table 1). Sentinel-2 products were used in this study because of the availability of higher spatial resolution and temporal resolution data, as compared to other satellites like Landsat.

Starting from December 3, 2015, the European Space Agency (ESA) has offered free access to Sentinel-2 Multispectral Instrument (MSI) imagery for users worldwide. The latest updated imagery can be freely obtained from the Copernicus Open Access Hub at (https://scihub.copernicus.eu). The Sentinel-2's multispectral imager (MSI) operates from an altitude of 786 km, capturing data across 13 different wavebands with a 290 km image width. Sentinel-2 has the revisit time of 10 days in the study area. The use of S2-MSI images has been common in monitoring lakes and rivers and in developing predictive models for Chl-a and turbidity (e.g., Sakuno et al., 2018; Soomets et al., 2020; Toming et al., 2016).

Table 1. Resolution and wavelengths of Sentinel 2 MSI bands

Spectral Bands	**Resolution**	**Wavelength**	**Description**
B1	60 m	443.9nm (S2A) / 442.3nm (S2B)	Aerosols
B2	10 m	496.6nm (S2A) / 492.1nm (S2B)	Blue
B3	10 m	560nm (S2A) / 559nm (S2B)	Green
B4	10 m	664.5nm (S2A) / 665nm (S2B)	Red
B5	20 m	703.9nm (S2A) / 703.8nm (S2B)	Red Edge 1

B6	20 m	740.2nm (S2A) / 739.1nm (S2B)	Red Edge 2
B7	20 m	782.5nm (S2A) / 779.7nm (S2B)	Red Edge 3
B8	10 m	835.1nm (S2A) / 833nm (S2B)	NIR
B8A	20 m	864.8nm (S2A) / 864nm (S2B)	Red Edge 4
B9	60 m	945nm (S2A) / 943.2nm (S2B)	Water vapor
B11	20 m	1613.7nm (S2A) / 1610.4nm (S2B)	SWIR 1
B12	20 m	2202.4nm (S2A) / 2185.7nm (S2B)	SWIR 2

This study utilized the Google Earth Engine (GEE) cloud computing platform to temporally match *in situ* water quality data with Sentinel-2 Level 2A (L2A) (ESA, 2024) satellite imagery. A series of iterations were run on *in situ* sample dates using GEE Python Application Programming Interface (API) to identify Sentinel-2 imagery corresponding to the exact date (or within 1 day) of *in situ* measurements for each water quality parameter. The time difference of a day was taken to maximize the matching samples. The matched imagery was resampled to a uniform spatial resolution of 30m across all spectral bands and band combinations. Resampling satellite images to a common spatial resolution is an important step in ensuring consistency and comparability across different spectral bands. To ensure the spatial representation of all spectral information aligns correctly all bands were resampled to a common resolution. The choice of 30m target resolution strikes a balance between the finer detail available in 10m bands and the broader coverage of 60m bands. Sentinel-2A bands at 10m resolution (e.g., visible bands like Blue, Green, Red, and Near-Infrared) provide high spatial detail, allowing for the detection of small-scale features. However, bands with 60m resolution offer broader spatial coverage but at the expense of finer detail. Resampling to 30m offers a compromise between these extremes, retaining significant spatial detail while providing a broader spatial context (Ahmed et al., 2022; Atkinson & Curran, 1997; Lillesand et al., 2015).

The spectral characteristics of Chl-a are most prominent in the blue (around 440 nm), red (around 665 nm), and green (around 550 nm) regions, while turbidity impacts reflectance particularly in the green and red bands. As bands with 60m resolution , bands 1 and 9 do not align with these key spectral regions and instead focus on atmospheric correction, resampling them to a higher or intermediate resolution, such as 30 meters, does not have prominent impact on the accuracy or effectiveness of water quality analysis (Lillesand et al., 2015). When resampling satellite imagery, several techniques can be employed, including nearest neighbor, bilinear interpolation, and cubic convolution. The choice of resampling technique depends on the specific requirements of the analysis and the characteristics of the data (Jensen & Lulla, 1987). The resampling of the images were performed using the Nearest Neighbor algorithm available in GEE Application Programming Interface (API). Nearest neighbor resampling technique was selected for the study because it preserves the original pixel values without any modifications (Li & Cheng, 2009). For water quality parameters such as Chl-a and turbidity, the exact reflectance values at specific wavelengths are critical. Any alteration through interpolation (such as in bilinear or cubic resampling) can introduce errors and reduce the accuracy of the analysis. Nearest neighbor resampling avoids the issue of artificial smoothing of pixel values by keeping the original pixel values intact, thus maintaining the distinct spectral signatures necessary for accurate measurement of water quality parameters (Jensen & Lulla, 1987). In addition, when integrating satellite data with ground-based observations, maintaining the original spectral integrity through nearest neighbor resampling enhances the accuracy of the correlation between the datasets (Lillesand et al., 2015). A total of 442 image collections (5304 image bands) for Chl-a and 481 image collection (5772 band images) were matched with the *in situ* samples between 2015 – 2023.

Combining raw satellite data from different wavelengths to create new indices like the Normalized Difference Chlorophyl Index (NDCI), Normalized Difference Turbidity Index (NDTI) and Green to Red ratio, has been shown to improve the accuracy in remote sensing applications (Kavzoglu & Bilucan, 2023). For each water quality variable, we selected a band combination based on previous studies as outlined in Table 2. A set of band combinations in the form of spectral indices will be computed and tested for Chl-a and turbidity parameters (Table 2). Previous studies have used multiple band ratios that show high correlation with the *in situ* samples as compared to studies exclusively utilizing band images. (Kavzoglu & Bilucan, 2023).

Table 2. Sentinel-2 band combinations for water quality parameters.

Parameters	Band Combinations	Ratios	References
Chl-a	Red to Green (RG)	B4/B3	(Cairo et al., 2019)
	Blue to Green (BG)	B2/B3	(O'Reilly & Werdell, 2019)

	Normalized Difference Chlorophyll Index (NDCI)	(B6-B5)/(B6+B5)	(Mishra & Mishra, 2012)
	Normalized Difference Vegetation Index (NDVI)	(B8-B4)/(B8+B4)	(Rouse et al., 1974)
	Green/Red	B3/B4	
	Green/Aerosols	B3/B1	
	Green/Blue	B3/B2	
	Red Edge 1/Red	B5/B4	
	Red Edge 2/Red	B6/B4	
	Red Edge 3/Red	B7/B4	
	Red Edge 4/ Red	B8A/B4	
	NIR/Red	B8/B4	
	Three Band Combination 1	(B5+B6)/B4	
	Three band Combination 2	((1/B4) - (1/B5))/B4	
Turbidity	Normalized Difference of Blue and Red (NDBR)	(B2-B4)/(B2+B4)	
	Normalized Difference of Red Edge 1 and NIR (NDRENIR)	(B5-B8)/(B5+B8)	
	Normalized Difference Turbidity Index (NDTI)	(B3-B8)/(B3+B8)	(Garg et al., 2020)
	Normalized Difference Vegetation Index (NDVI)	(B8-B4)/(B8+B4)	(Rouse et al., 1974)

5.4. Pre-Processing and Data Split

Pre-processing techniques are the image preparation and the processing operations carried out before analysis to correct or minimize image distortions from, i.e., imaging systems, sensors, and observing conditions (Peterson et al., 2020). Cloud masking operation is crucial for removing unwanted atmospheric interference, ensuring the accuracy of subsequent analyses. We used the Quality Assessment (QA) band to identify pixels containing clouds, cirrus, or shadows. Bitwise operations were used to create a mask, retaining only those pixels where none of these atmospheric conditions were detected. To normalize the mask values for practical use in analyses, the mask was scaled by dividing by 1000. This scaling ensures that the mask values are within a manageable numerical range. Proper scaling ensures that different features within the data are weighted appropriately for analysis, leading to more accurate interpretations. . The mathematical representation of the mask is represented in Equation 1 (Gandhi, 2023):

$$mask = QA.bitwiseAnd(cloudBitMask) \\ = 0 \ AND \ QA.bitwiseAnd(cirrusBitMask) = 0 \quad (1)$$

where:

QA = quality assessment band of the input image
$cloudBitMask$ = bit masks for clouds
$cirrusBitMask$ = bit masks for cirrus clouds

Following data preprocessing, a data splitting procedure was implemented. This was done to mitigate the risk of overfitting in the developed model, as emphasized by Nguyen et al. (2021). In line with established best practices, we adopted a common partition ratio of 70/30 for pairwise surface reflectance values and *in situ* samples, as recommended by (Zhang et al., 2022).

The existence of some patterns that significantly deviate from the bulk of sample cases is a common problem in machine learning. These data samples are often referred to as outliers. These points can skew the model training and can result in less accurate predictions. It is important to identify and remove them before building any supervised model and this is the first step when dealing with machine learning problem (Fernández et al., 2022). The Gaussian-method based on box plot was used to identify and remove the outliers from *in situ* data samples (Owuor et al., 2022). An outlier threshold of 100 µg/L was set for Chl-a whereas 140 NTU was set for Turbidity. Similarly, for the feature variables outliers were detected using Isolation Forest technique (Liu et al., 2008). The contamination parameter in Isolation Forest estimates the proportion of outliers in your data, influencing the threshold for flagging anomalies (Al Farizi et al., 2021). The contamination parameter of the isolation forest was set to 0.05 indicating approximately 5% of the data points are expected to be outliers given the data was accurately extracted using Google Earth Engine. This process involves building an ensemble of isolated trees to learn the patterns in the data and detect anomalies. The fitted Isolation Forest model was then used to predict outliers in the feature dataset. A total of 33 datasets were removed as outliers from samples corresponding to Chl-a variables and 46 samples were removed from the samples corresponding to turbidity variables.

A total of 442 Chl-a samples and 481 turbidity samples with corresponding surface reflectance values and auxiliary variables were used for model training and testing purpose. The Chl-a values ranged from 3.46 µg/L to 76.6 µg/L whereas turbidity values ranged from 4.1 NTU to 134 NTU. The summary of data used for model training and testing is outlined in Table 3.

Table 3. Descriptive statistics of chlorophyll-a (Chl-a) and turbidity measurements in water samples, including mean, standard deviation (SD), minimum, 25th percentile, median, 75th percentile, and maximum values.

	N	Mean	SD	Min	25%	50%	75%	Max
Chl-a	442	14.28	10.32	3.46	7.15	10.6	18.72	76.6
Turbidity	481	29.92	24.48	4.1	11.4	22.4	39.3	134

Since the log transformed in situ Chl-a and turbidity data were close to a normal distribution as shown in Figure 5, standardization of all the features was performed using a standard scaler to remove bias in model fitting (Al-Imam, 2019; Curran-Everett, 2018; Garreta & Moncecchi, 2013; Ha et al., 2021). The summary of data structure before and after log transformation is shown in Figure 5.

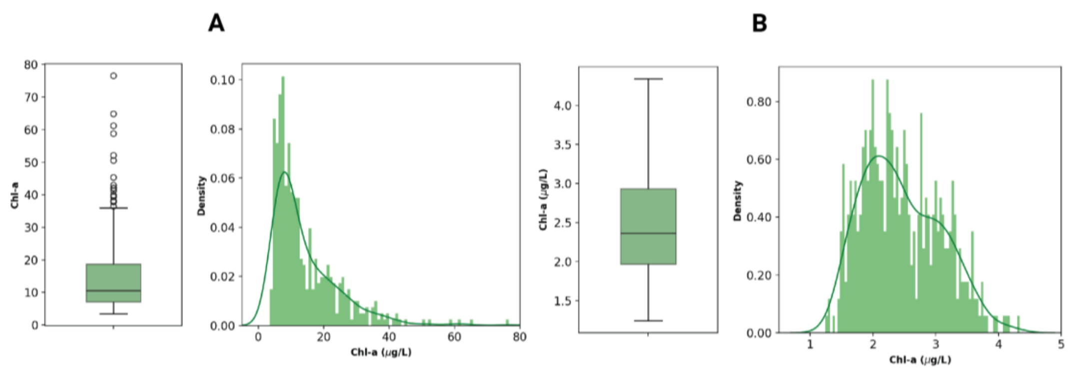

Figure 6 Whisker and distribution plots of in situ water quality parameters before (A) and after (B) log transformation for Chl-a

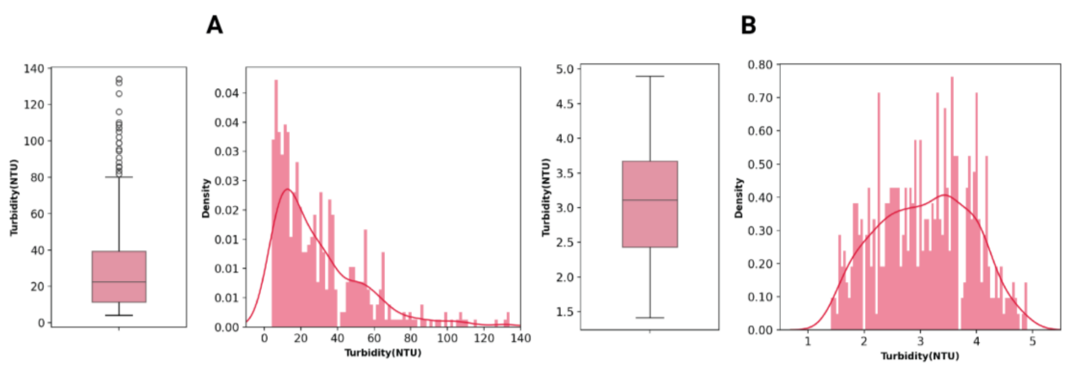

Figure 7. Whisker and distribution plots of in situ water quality parameters before (A) and after (B) log transformation for turbidity

5.5. Classical Machine Learning (ML) Models

Machine learning algorithms have been found to be superior in coping with high-dimensional, nonlinear regression problems (Chen et al., 2019). In general, classical ML models can be classified into two types: tree-based models and generalized linear classifier-based models. In this study, we choose Random Forest Regression (RF) and Support Vector Regression (SVR) as representative algorithms for each type of ML model respectively as the representative for each type.

5.5.1. Support Vector Regression (SVR)

Support Vector Machine (SVM), the foundation of Support Vector Regression (SVR), is a type of supervised machine learning algorithm that provides analysis of data for classification and regression analyses. Although they are predominantly recognized for their classification capabilities, they are also widely used for performing regression-based analysis. SVR constructs optimal separating hyperplanes between classes in feature space using support vectors. An optimal hyperplane is a decision surface that can separate classes from each other with maximum margin, and support vectors are the data points nearest to the hyperplane that are most difficult. SVR contains polynomial functions radial basis function (RBF) networks as special cases (Scholkopf et al., 1997).

Given a set of training data $\{(x_1, y_1), \ldots, (x_n, y_n)\} \subset \chi \in \mathbb{R}$, where χ denotes the space of the input feature dataset comprising surface reflectance band values and auxiliary variables, and yi represents the water quality measurements. The objective is to find a function $y=\langle w, x\rangle+b$, $w \in \chi$, $b \in \mathbb{R}$ that has a maximum deviation ε from the real measured targets yi for all the training data and, simultaneously, is as flat as possible. In case of linear function in SVR, we can express convex optimization problem as the minimization of the Euclidean norm making sure we deal with infeasible constraints using slack variables ξ_i, ξ^*. Slack variables are introduced to allow certain constraints to be violated (Haifeng Wang & Dejin Hu, 2005). After introducing the slack variable we reach the condition stated by (Vapnik, 1999):

$$minimize: \frac{1}{2}\,||w||^2 + C\sum_{i=1}^{n}(\xi_i + \xi_i^*) \qquad (1.1)$$

$$subject\ to: \begin{cases} y_i - (w, x_i) - b \leq \varepsilon + \xi_i \\ (w, x_i) + b - y_i \leq \varepsilon + \xi_i^* \\ \varepsilon + \xi_i^* \geq 0 \end{cases} \tag{1.2}$$

where constant $C > 0$ is a fixed penalty parameter. Since the surface reflectance values and derived band ratios, we are using are in non-linear form we need to expand the SVR capability to non-linear functions. When dealing with non-linear functions, we express the optimization problem in its dual form by using a Lagrange function that incorporates both the objective function and the associated constraints, while introducing a set of dual variables. A condition is reached:

$$y = \sum_{i=1}^{n} (\alpha_i - \alpha_i^*)(x_i, x) + b \tag{1.3}$$

where α_i *and* α_i^* are Lagrange multipliers associated with the support vectors, x_i are the input data points and b is the bias term in SVR model. To handle the non-linear problems in a computationally efficient manner "kernel trick" is introduced. The kernel functions transform the data into a higher dimensional feature space to make it possible to perform the linear separation(Y. Chen et al., 2017). The outcome can be written as:

$$y = \sum_{i=1}^{n} (\alpha_i - \alpha_i^*). K(x_i, x) + b \tag{1.4}$$

where K (x_i, x) is the non-linear function called kernel. To transform the data to higher dimensional feature space there are mainly two types of kernel functions: polynomial and radial basis functions which are expressed as below:

$$Polynomial\ Function: K(x_i, x_j) = (x_i . x_j)^d \tag{1.5}$$

$$Gaussian\ Radial\ Basis\ Function: K(x_i, x_j) = exp\left(- \frac{||x_i\ -\ x_j||^2}{2\sigma^2}\right) \tag{1.6}$$

where d is the degree of polynomial and σ is a positive constant called scale parameter. Both polynomial and radial basis function were trained and tuned for the best hyper parameters C, d and σ was done to find the best hyperplane to predict the water quality parameters.

5.5.2. Random Forest Regression (RF)

Decision tree is the basic structure of many ensemble learning methods, called classification tree when used for classification and regression tree when used for regression (Loh, 2011). Random Forest Regression is an algorithm based on the regression tree proposed by (Breiman, 2001). The main idea is to improve the prediction accuracy of the model by summarizing multiple regression trees. By randomly selecting sample features, the correlation between decision trees is reduced, and the correlation between decision trees is small, so as to further improve the accuracy of the model (Tian et al., 2022). Random Forest builds T decision trees, each trained on a bootstrapped dataset. For a given input of surface reflectance band values and auxiliary data as x_i, the prediction i.e. actual water quality measurements $\hat{y}_i$ from one decision tree is computed as:

$$\hat{y}_i^{(t)} = \frac{1}{N_t} \sum\nolimits_{x_j \in leaf(x_i)} y_j \tag{2.1}$$

where t represents tree, N_t is number of data points in leaf node $leaf(x_i)$ represents the leaf node that xi falls into the t-th tree. The final prediction from Random Forest is average of the prediction from all individual trees represented as:

$$\hat{y}_i = \frac{1}{T} \sum_{t=1}^{T} \hat{y}_i^{(t)} \tag{2.2}$$

where T represents the total number of trees in random forest. The performance of the model was evaluated based on predictive capability. The hyperparameters like number of trees (NT) and maximum depth were tuned to minimize the Out of Bag (OOB) error rate of the model. The OOB error rate is the average prediction error for each training sample, calculated using only the trees in the Random Forest that did not include the sample in their bootstrap sample. It serves as an unbiased estimate of the model's prediction error (Breiman, 2001).

5.6. Deep Neural Network Regression (DNN)

DNN, also known as a feedforward neural network or multilayer perceptron, is a fundamental neural network architecture (Rolnick & Tegmark, 2017). Many complex regression or classification problems cannot be solved with a single hidden layer, so we must increase the depth of the network by setting multiple hidden layers. As the multiple hidden layer network architecture has a better ability to represent the data, it can extract deeper features to potentially improve the accuracy of the regression and classification and can learn patterns from the input data (Niu et al., 2021). In regression tasks, the goal is to find a non-linear function that maps input data to a continuous output space.

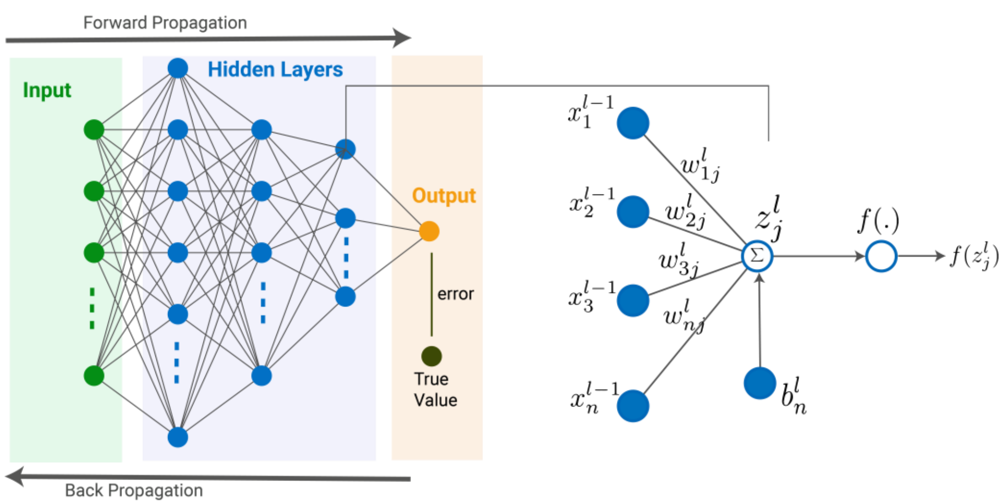

Figure 8. Architecture of a Deep Neural Network

The basic structure of an artificial neural network involves a network of many interconnected neurons in between hidden layers. These neurons are very simple processing elements that individually combine pieces of one big problem. As presented in the figure above each neuron in the *l*th layer must be connected to any neuron in the $l + 1$st layer and the following equation indicates the nonlinear relationship between the DNN layers shown in figure 4.

$$a_j^{l+1} = f\left(\sum_{i=1}^{n} a_i^l \, w_{ij}^l + b_j^l\right) \tag{3.1}$$

where a_i^l is the activation value of the ith node in the lth layer, a_j^{l+1} is the activation value of the *j*th node in the *l + 1*st layer, w_{ij}^l is the weight between a_i^l and a_j^{l+1}, b_j^l is the bias value of *j*th neuron in *l+1* st layer (Qian et al., 2022).

Each neuron computes one output using an activation function that considers the weighted sum of all its inputs (Muharemi et al., 2019). The most common activation function is Rectified Linear Unit (ReLU). The main purpose of this function is to introduce the property of nonlinearity into the model. The ReLU function is defined as:

$$f(x) = max\,(0, x) \tag{3.2}$$

where, f(x) is the output of ReLU and x is the input signal. It is observed that ReLU improves the computational speed and accuracy compared with the other activation functions (e.g., sigmoid function)(Nair & Hinton, 2010). Since the non-linearity of surface reflectance values and band ratios and computational advantage, ReLU was employed as the activation function for this study. A method for stochastic optimization, namely ADAM (Adaptive Moment Estimation) was utilized for training deep learning models i.e. to update network weights iterative in training data. ADAM is one of the algorithms that work well in a range of deep learning architectures

Dropout regularization technique was used for both models to prevent overfitting issues. Dropout is one of the most popular regularization methods in the scholarly domain for preventing a neural network model from overfitting in the training phase (Salehin & Kang, 2023). The dropout technique randomly deactivates a chosen proportion of neurons (and their connections) within a layer. To compensate for the deactivated neurons, the outputs of the remaining active neurons are scaled by a factor corresponding to the probability of each neuron being active (Wager et al., 2013). After several iterations, a dropout of 20% was adopted to both the models.

For Chl-a, the input dimension was 25 and first dense layer consisted of 256 neurons. The model consisted of five hidden layers and the number of neurons decreased exponentially by a factor of 2 for each hidden layer and a dropout layer in between. Each hidden layer used the ReLU activation function. A Dropout layer with a 20% dropout rate was added after each hidden layer to prevent overfitting. For turbidity, the input dimension was 19 and the first dense layer consisted of 128 neurons. The model consisted of four hidden layers with the number of neurons decreasing exponentially by a factor of 2 for each hidden layer and a dropout layer in between. Each hidden layer used the ReLU activation function. A Dropout layer with a 20% dropout rate was added after each hidden layer to prevent overfitting. Both models used Mean Squared Error (MSE) as the loss function and Mean Absolute Error (MAE) as evaluation metric. ADAM optimizer was used to minimize the loss function. Adam dynamically adjusted the learning rate based on the first and second moment estimates of the gradients, leading to efficient and effective training. To ensure balanced model without overfitting DNN model for Chl-a was trained to 200 steps and DNN model for turbidity was trained to 300 steps.

5.7. Model evaluation and comparison

The coefficient of determination (R^2), the root mean square error (RMSE), mean relative error (MRE) and Mean Absolute Error (MAE) were used as the accuracy evaluation metrics to assess and validate the performance of the proposed models and select the most suitable one (H. Yang, Du, et al., 2022).

$$R^2 = 1 - \frac{\sum_{i=1}^{n}(Y_i - \hat{Y}_i)^2}{\sum_{i=1}^{n}(Y_i - \bar{Y}_i)^2} \tag{4.1}$$

$$RMSE = \sqrt{\frac{\sum_{i=1}^{n}(\hat{Y}_i - Y_i)^2}{n}} \tag{4.2}$$

$$MRE = \frac{1}{n}\sum_{i=1}^{n}\frac{||\hat{Y}_i - Y_i||}{Y_i}.100\% \tag{4.3}$$

$$MAE = \frac{\sum_{i=1}^{n}\hat{Y}_i - Y_i}{n} \tag{4.4}$$

where Y_i is the actual value, $\hat{Y}_i$ is the predicted value, $\bar{Y}_i$ arithmetic mean of the sampled data and n is the total number of samples. The coefficient of determination (R^2) can be interpreted as the proportion of the variance in the dependent variable that is predictable from the independent variables. The root mean square error (RMSE) is a measure of the differences between predicted and actual values in a regression analysis (Chicco et al., 2021). Mean relative error (MRE) is a measure of the average magnitude of the relative errors between a set of predicted values and their actual values. It is calculated as the mean of the relative errors, where each relative error is the ratio of the absolute error to the actual value(Stensrud et al., 2002).

5.8. Map Generation

The final step involved generating the predicted maps of Chl-a concentration and turbidity for the study area. We utilized the Google Earth Engine Python Application Programming Interface (API) to create a composite image composed of 12 spectral bands, three true color images from the red, green, and blue channels and auxiliary ratios and indices. The study area has two primary seasons: the wet season and the dry season, as explained in the study area section. To represent these seasonal variations, two mean monthly composites were developed, corresponding to January 2021 for the dry season and July 2021 for the wet season. The image composites for Chl-a and turbidity had 25 and 19 bands corresponding to the feature variables. All the bands were converted to a two-dimensional array and best fit RF, SVR and DNN models were run respectively for both water quality parameters. The predicted two-dimensional array was assigned to the original coordinate reference system (CRS) and plotted to create predicted Chl-a and turbidity maps for wet and dry season for all the models.

6. Results

6.1. Regression Models Results

The results of the regression models are displayed in Table 4. The proposed exponentially decreasing deep neural network (DNN) approach produced results with higher R^2 values, and lower MSE, RMSE, MRE, and MAE values than classical ML models. When applied to test dataset, the DNN approach showed a higher correlation with (R^2=0.62, MSE=0.14, RMSE=0.38, MRE=12.15%, MAE=0.30) for Chl-a and (R^2=0.72, MSE=0.14, RMSE=0.37, MRE=9.60%, MAE=0.28) for turbidity. RF performed slightly better than SVR for both Chl-a and turbidity, except for MRE in turbidity prediction. SVR has the lowest performance among the three models in predicting both parameters across all metrices. For the Chl-a parameter, the DNN approach outperformed the RF model by 12.7% and the SVR model by 16.9% when assessed using R^2. Similarly, for the Turbidity parameter the DNN approach outperformed the RF model by 18.03% and the SVR model by 28.5% when assessed using R^2. With relatively minor variations between training and testing outcomes, the DNN approach also showed a minimal degree of overfitting as compared to other models.

Table 4. Results of the regression models between Sentinel-2 MSI derived surface reflectance and the corresponding in situ station water quality data in log transformed test dataset with target variables Chl-a in NTU and turbidity in µg/L . Highlighted in bold are the best model results for each sensor when applied to testing dataset.

Model	Parameter	R^2	MSE	RMSE	MRE	MAE
SVR	Chl-a	0.53	0.18	0.42	24.27%	0.34
	Turbidity	0.56	0.21	0.46	23.63%	0.38
RF	Chl-a	0.55	0.17	0.41	24.34%	0.34
	Turbidity	0.61	0.19	0.44	24.99%	0.35
DNN	Chl-a	**0.62**	**0.14**	**0.38**	**12.15%**	**0.30**
	Turbidity	**0.72**	**0.14**	**0.37**	**9.60%**	**0.28**

The plotted results for all three models for each water quality variable are shown in Figure 9. Overall, the models successfully predicted a range of variable concentrations. The results indicate that the models developed for Chl-a and turbidity exhibited greater error in predicting lower values (<log(2.5)). The point cluster is tighter around the diagonal for DNN models whereas more spread is seen in other models. As seen in the figure, there are more dense clusters around the diagonal line in DNN model. Also, the distribution of points is more symmetrical around the diagonal line for DNN model suggesting that the model underestimates and overestimates the concentration with similar frequency. Although there is some bias towards underestimation and overestimation in the DNN models, this trend is more prominent in RF and SVR models. A tighter cluster, symmetrical spread, higher R^2 and lower error metrices of the DNN model confirm that model is superior in predicting optically active water quality parameters as compared to other classical machine learning model and auxiliary and ancillary band variables.

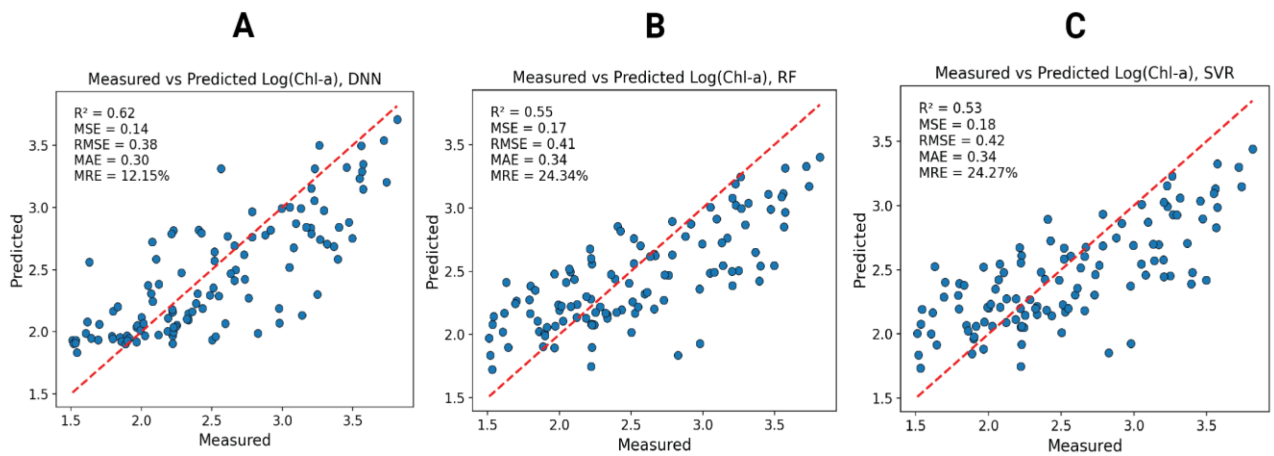

Figure 9. Plots of the observed versus predicted Chl-a maps when using DNN(A), RF(B) and SVR(C. Each panel (A, B, and C) displays a scatter plot showing the relationship between the measured Chl-a concentrations (x-axis) and the Chl-a concentrations predicted by each model (y-axis).

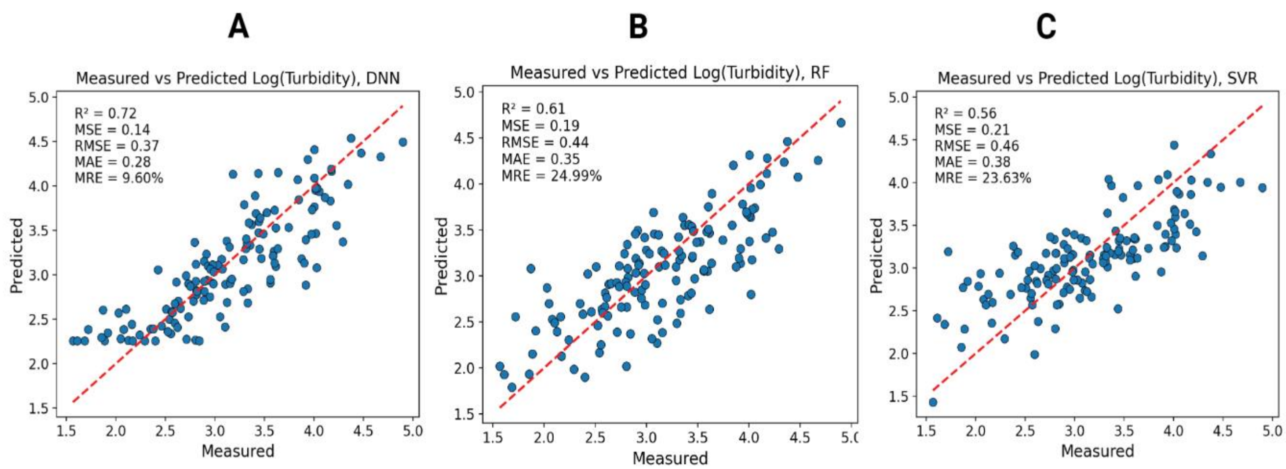

Figure 10. Plots of the observed versus predicted Chl-a maps when using DNN(A), RF(B) and SVR(C). Each panel (A, B, and C) displays a scatter plot showing the relationship between the measured turbidity concentrations (x-axis) and the turbidity concentrations predicted by each model (y-axis)

Overall, the DNN model demonstrated strong performance for retrieving optically active water quality parameters like Chl-a and Turbidity. While the accuracy of the model might be moderate when directly applied to other in land lake areas, the modeling process is straightforward and can be easily calibrated by retraining the model with new data for any specific region. Therefore, the proposed methodology demonstrates high transferability and can be effectively applied across various regions.

6.2. Performance Tuning of DNN Models

Training loss, which is represented by blue curve in Figure 11 measures how well the model fits with the training data over the successive epochs. Initially, the observed elevation in loss can be due to the parameter adjustment within the model. This initial phase of training typically entails larger fluctuations in loss values, reflecting the model's adaptation process to the training data. As training progressed, the training loss steadily decreased, indicating that the model is learning and improving its ability to make predictions on the training data. The orange line in Figure 11 represents the validation loss, which evaluates the model's performance on a separate validation dataset that it hasn't seen during training.

The initial decrease in validation loss indicated that the model was effective in generalizing the unseen data, as evidenced by the reduction in loss on the validation dataset in both Chl-a and turbidity model. In steps 1 to 75 for Chl-a and steps 1 to 150 for turbidity the models were not generalizing the unseen data very well but after that the validation loss started to converge with the training loss indicating that there was no overfitting issue. A similar trend was seen in the MAE curve that showed the absolute error on training data and validation dataset started to converge around step 125 for Chl-a and 250 for turbidity and the trend continued thereafter. The training was stopped at step 200 for Chl-a and 300 for turbidity as no significant improvement on loss and MAE was observed. Hence, the models reached the optimum state at step 200 and 300 respectively.

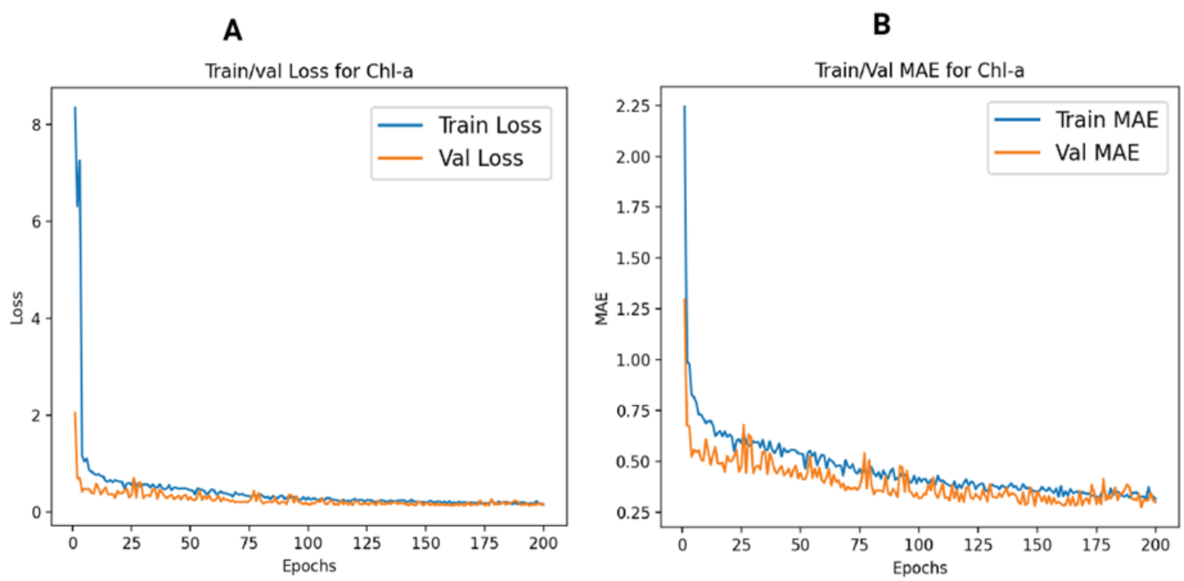

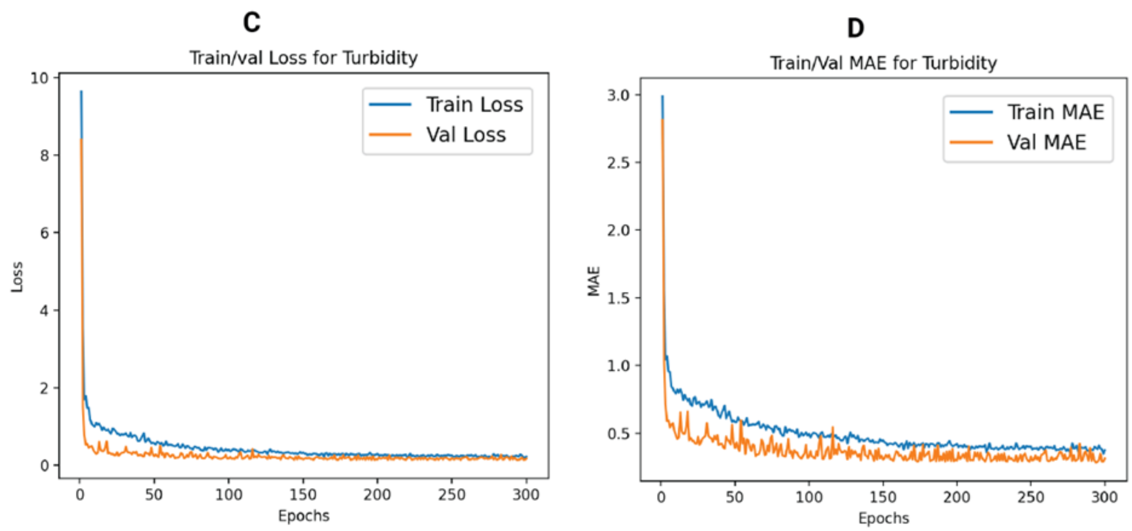

Figure 11 Training and validation loss and MAE for Chl-a (A and B respectively), training and validation loss and MAE for turbidity (C and D respectively)

6.3. Performance Tuning of RF Model

The impact of the number of trees (NT) parameter on prediction performance based on the input spectral bands and auxiliary data was analyzed for the study area for both water quality parameters. The optimal NT hyperparameter was determined by minimizing the out-of-bag (OOB) error rate, starting from one tree with a step size of one up to 300. The OOB errors varied from 7.29 to 0.67 for the Chl-a and 2.24 to 0.46 for the Turbidity. The OOB errors were quite high at first in the range of 1 to 30 and did not alter significantly after step 100. As the number of trees increases the model complexity increases and vice versa. We opted for NT of 300 to achieve a balance between error reduction and computational time because the OOB errors did not change much after increasing the NT to 200 and 300 as represented in Figure 12.

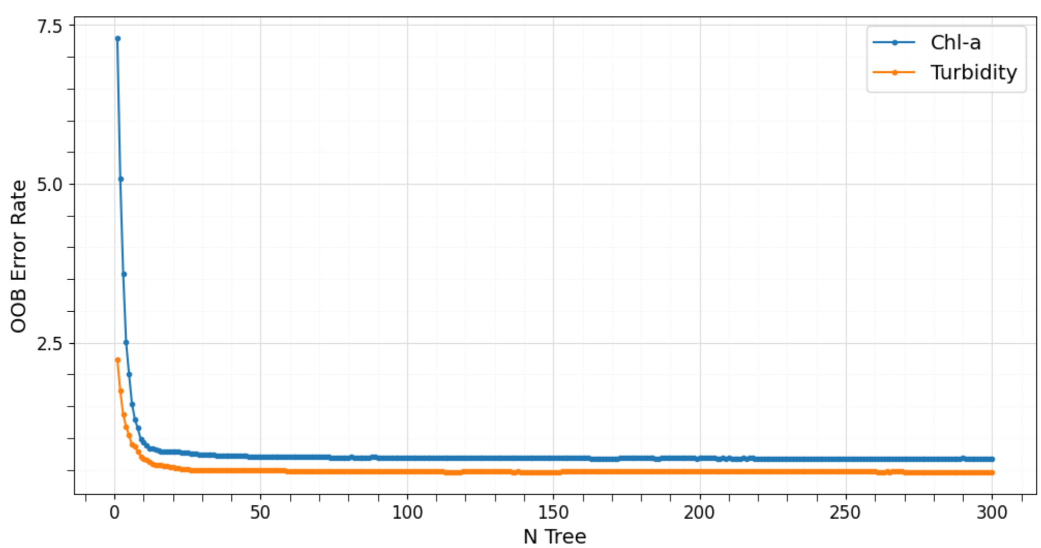

Figure 12. Trend of Out of Bag (OOB) error rate with increase in number of trees in RF model for Chl-a (blue) and turbidity (orange)

The layout of the split variables in a decision tree provides information about the importance of the features in the general classification model and in the classification of each category (Pal & Mather, 2003).

After performing RF classification, variable importance for each input feature was calculated. Figure 13 represents the feature importances for the models used for Chl-a and turbidity. The feature importance for a random forest is a measure of the contribution of each feature to the overall prediction accuracy of the model. It is calculated based on the decrease in impurity (e.g., Gini impurity for classification or mean squared error for regression) brought by a feature, averaging over all the trees in the forest. Among the twelve spectral bands Sentinel 2A and the ancillary variables, NDCI was the most influential for Chl-a and NDTI was most influential in Turbidity. This highlights the importance of ancillary variables prediction task. NDCI, B9, B11, B3 and NDVI were the most influential for Chl-a whereas NDTI, B11, NDBR, B12 and B4 were among the most influential features for Turbidity as shown in Fig 13.

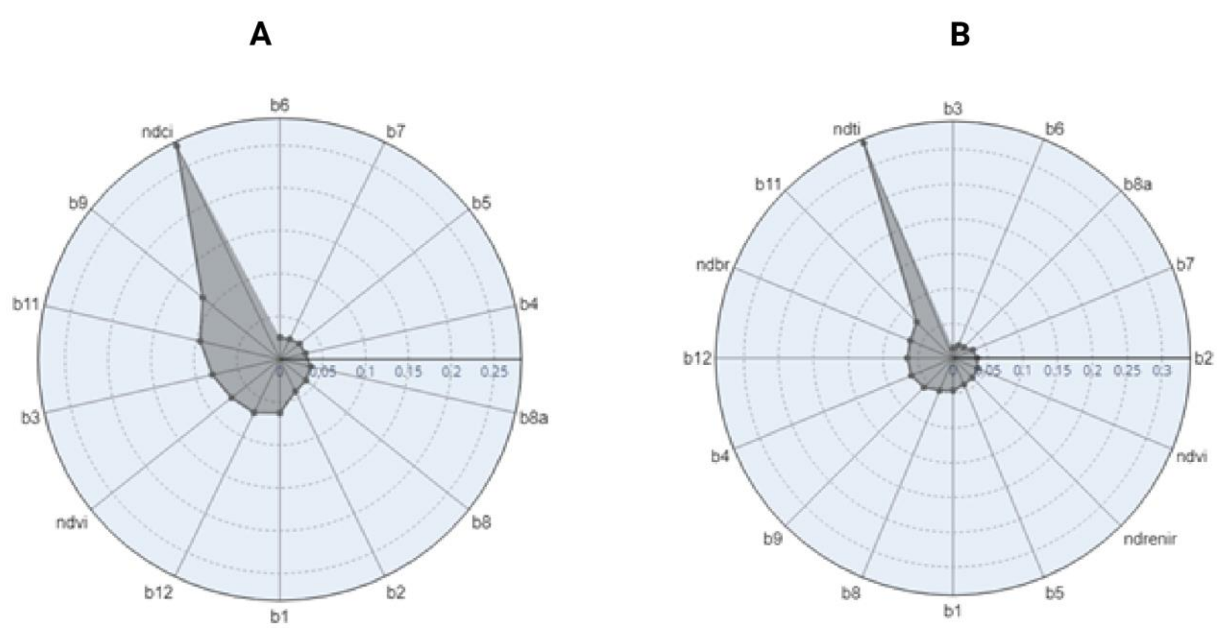

Figure 13 Variable importance contribution of spectral band variables and ancillary variables for Chl-a (A) and turbidity (B)

6.4. Mapping of water quality variables in Lake Okeechobee

We effectively mapped water quality parameters over Lake Okeechobee, minimizing the need for physical sampling and localized lab analyses. As discussed in results above the proposed mapping technique showed superiority over traditional techniques like empirical statistical models, band ratio algorithms and spatial interpolation techniques (Ahmed et al., 2022; El Ouali et al., 2021; Murphy et al., 2010; Toming et al., 2016; H. Yang, Kong, et al., 2022). The spatial distribution maps of Chl-a and turbidity from of two monthly average surface reflectance, one for the dry season (January 2021) and one for a wet season (July 2021) were produced by applying all three models. Subsequently, we mapped the spatial distributions of monthly mean Chl-a and turbidity in Lake Okeechobee for January 2021 and July 2021. According to the best-fit model Chl-a concentrations ranged from 4.86 μg/L to 123.10 μg/L in the month of July and log 4.86 μg/L to 123.10 μg/L in the month of January. Similarly, turbidity concentrations ranged from 6.04 NTU to 148 NTU for January and 4.48 NTU to 270 NTU for July. From the maps, it could be observed that the concentrations of Chl-a and turbidity are not evenly distributed. Turbidity is more concentrated in lower middle part of the lake for both months and whereas very sparse on the edges whereas Chl-a was prominent in the western edge and the center. The unique pattern of Chl-a concentration at the western edges can be attributed to inflow of the nutrient and pollutants rivers merging in the lake in that region (Canfield & Hoyer, 1988).

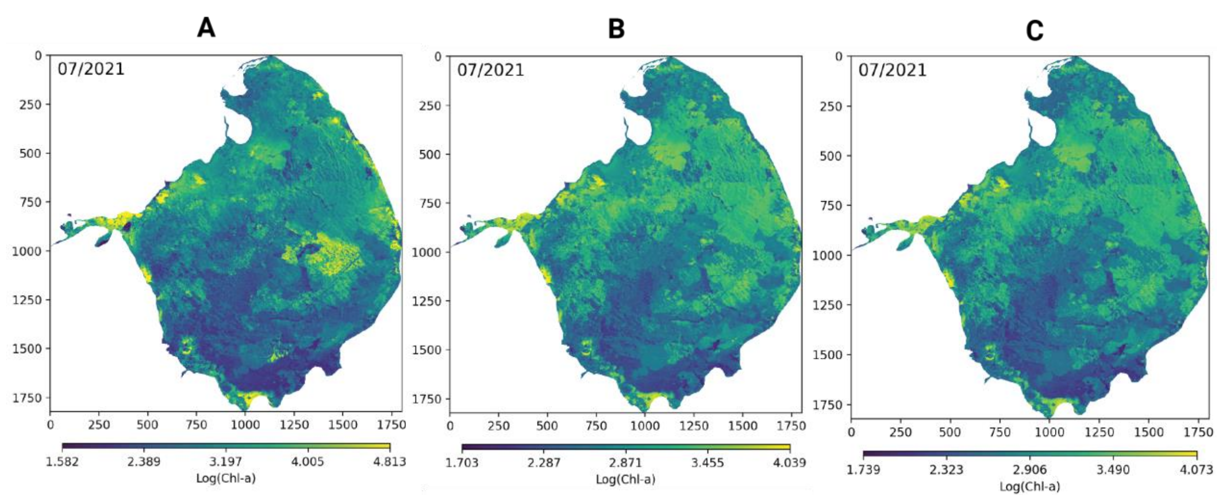

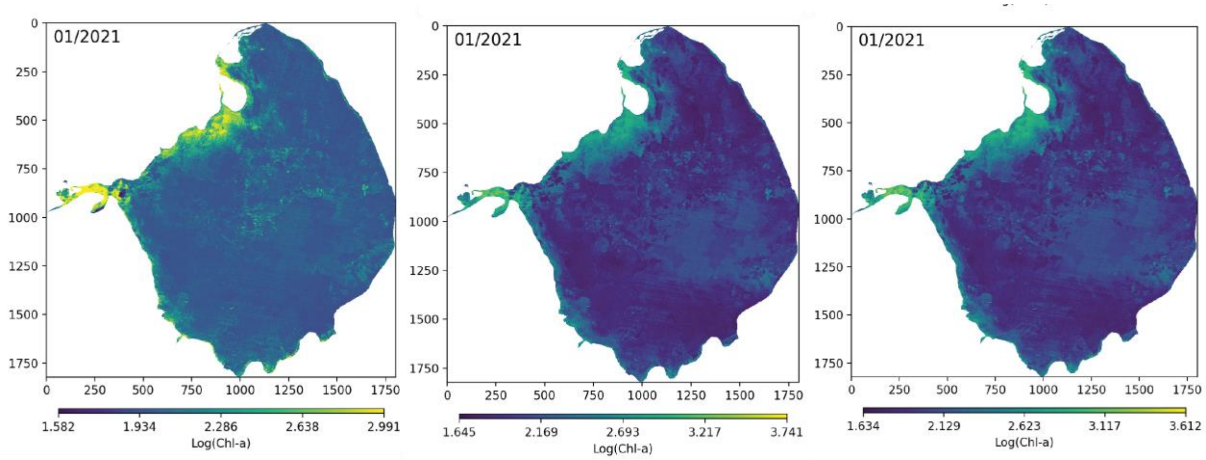

Figure 14. The monthly variability of Chl-a for July 2021 (first row) and January 2021 (second row) as predicted by different models A, B and C. A = DNN, B = RF and C = SVR

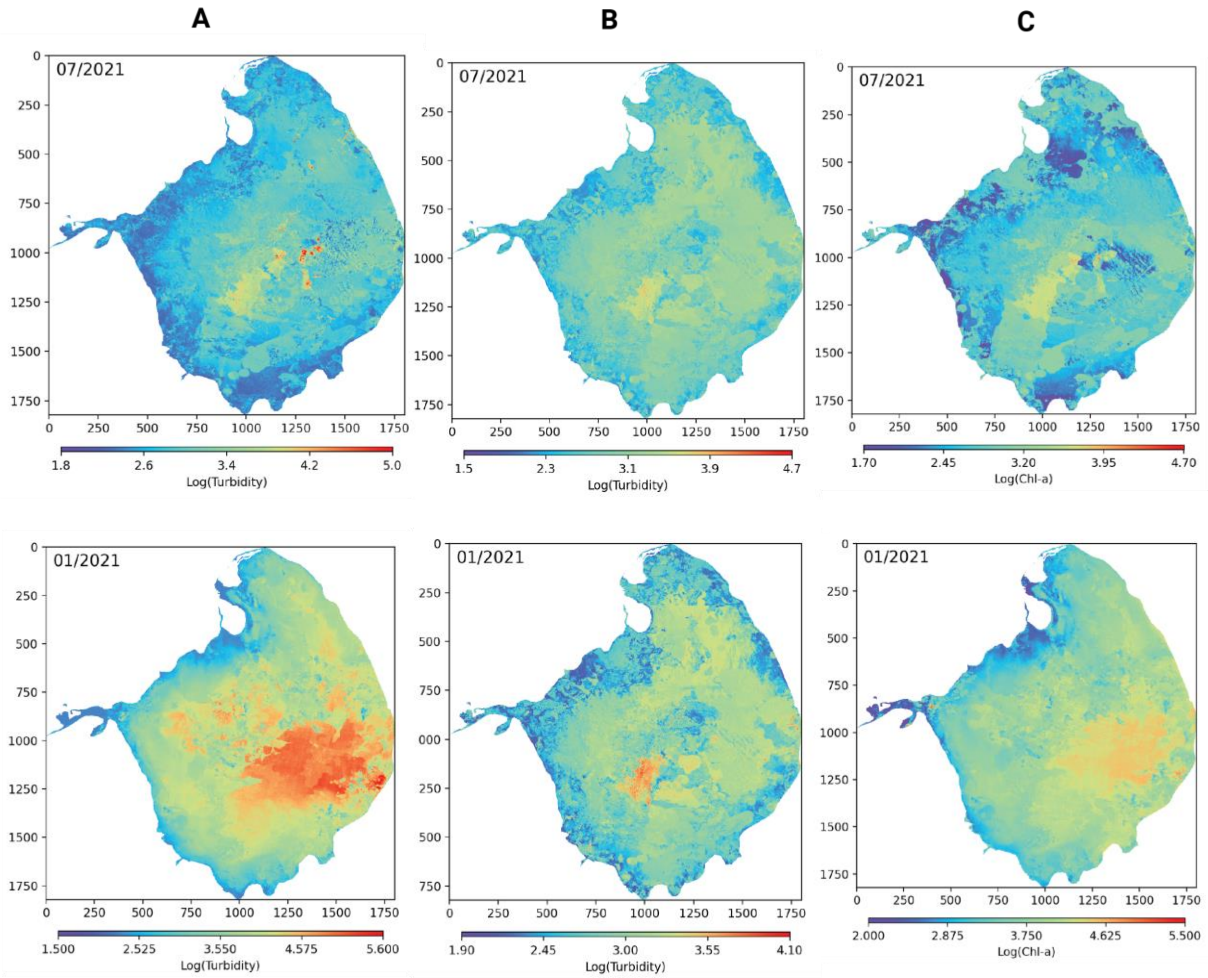

Figure 15. The monthly variability of turbidity for July 2021 (first row) and January 2021 (second row) as predicted by different models A, B and C. A = DNN, B = RF and C = SVR

7. Discussion

7.1. Remote Sensing for Water Quality

With the rise in number of new satellites and multi-sensor/platform remote sensing data over the past decade, water quality monitoring has advanced rapidly (Chen et al., 2022). Among satellite data products that can be used for water quality assessment, we choose Sentinel-2 for this study because of its higher spatial resolution, frequent revisit times, large coverage, consistency, and reliability (Phiri et al., 2020; Solórzano et al., 2021). Sentinel 2 MSI sensors have been used successfully to measure most of the important water quality parameters like Chlorophyll-a, turbidity, and Total Suspended Solids (TSS) (Ouma et al., 2020). Given similar data source, add more information about those studies; modeling techniques used, and accuracies achieved.

Most of the previous studies are either based on band indices or conventional regression techniques that fail to capture complex non-linear relationship between image band values and water quality parameters (Akbar et al., 2014; Yigit Avdan et al., 2019; F. Zhang et al., 2021). Previous research has relied on empirical relationships between satellite-derived reflectance and target water quality parameters to apply relatively simple linear or nonlinear regressions on satellite data. The empirical models produced have a limitation in that they may not operate effectively in diverse environments (such as the open ocean, coastal, river or inland waters) (Hassan & Woo, 2021).

7.2. Methodological Highlights

We studied different machine learning and deep learning approaches for water quality retrieval. The water quality data used in this study were acquired over the course of 2015-2023 providing a robust picture of regional water quality trends. The use of remote sensing for water quality analysis is growing, as it offers advantages over traditional *in situ* methods. We used Sentinel-2 satellite imagery which is one of the popular open source remote sensing imagery for studying optically active water quality parameters. To ensure consistency across different bands of the satellite imagery resampling was performed by balancing detail from 10m bands and coverage from 60m bands. The Nearest Neighbor algorithm was chosen for resampling because it preserves original pixel values and spectral integrity, which is crucial for accurate water quality analysis. Another crucial step before training the models on training data was to detect the potential anomalies in the dataset. To identify and eliminate anomalies in the feature dataset, we employed Isolation Forest (Liu et al., 2008) techniques. This method effectively isolates outliers by constructing an ensemble of trees and identifying instances with shorter path lengths as anomalies. Additionally, extreme values of Chl-a and turbidity were excluded from the dataset. These outliers have the potential to adversely affect model performance and introduce bias, thereby compromising the integrity of the results. For a comprehensive evaluation of the performance of the machine learning and deep learning model for water quality parameters retrieval, we compared the performances of the DNN model, random forest (RF) model, and support vector (SVR) model based on accuracy metrices like R^2 and error metrices like MSE, RMSE, MRE and MAE. Our results clearly showed the advantages of using deep learning methods over traditional machine learning approaches. In addition to the generalizability of the DNN approach there was also noticeably lower overfitting when compared to the other methods. The degree of overfitting can often be related to a very high number of trainable parameters within the network. Several steps were taken in the design of the DNN architecture to reduce issues of overfitting including limiting the number of processing nodes within each hidden layer, utilizing early stopping during model training, and the use of regularization in the backpropagation paradigm which has been proven to reduce model overfitting (Nielsen, 2015).

Overall, the application of the developed water quality estimation method in the test cases demonstrated the effectiveness for quantifying and visualizing the spatial trends for a range of variables. We were able to map the distribution of water quality parameters across the lake using the developed regression models. We converted each spectral bands from Sentinel-2 imagery to a two-dimensional array and ran the RF, SVR, and DNN models to predict the water quality parameters, then mapped the predictions to the original coordinate reference system to visualize the spatial distribution. This method of mapping water quality variables provides a fact and effective way to map the water quality parameters across large spatial areas, reducing reliance on physical sampling and localized lab analysis. This advancement in water quality monitoring holds significant potential for improving the management and conservation of aquatic ecosystems, enabling more informed decision-making and effective environmental protection strategies.

Some of the limitations of this study come from the time delta between the satellite observations and ground sampling dates. We took a time interval of ± one day to maximize the sample size. Several influencing factors like human activities near the sample location and wind speed during the time interval can also play a vital role. Implementing an automated system using the techniques outlined in this study could lead to the creation of an advanced water quality monitoring system.

This would empower water resource managers and researchers to address and respond to water quality issues more effectively.

8. Conclusions

Satellite imagery captured using Sentiel-2 MSI sensor was coupled with ground sampling measurements of two major optically active water quality parameters: Chl-a and turbidity. Introducing a time delta of three days significantly improved the temporal frequency of the dataset which is required for a complex inland water system like Lake Okeechobee. We developed and tested two classical machine learning and deep neural network-based regression techniques to automatically predict water quality parameters based on surface reflectance values. The proposed Deep Neural Network Regression (DNN) showed a robust estimation accuracy across both water quality parameters. It significantly outperformed classical techniques like Random Forest Regression (RF) and Support Vector Regression (SVR). Applying the proposed DNN technique to available Sentinel -2 dataset for the study area gave a predicted Chl-a and turbidity and can be adopted and calibrated to other locations.

9. Research Highlights

- Coupled Sentinel 2 MSI Level 2A Surface Reflectance with *in situ* samples
- Developed robust deep learning technique to estimate water quality parameters cost effective remote sensing technique that can be calibrated other locations
- Predicted water quality variable maps for greater spatial and temporal context

10. References

Adusei, Y. Y., Quaye-Ballard, J., Adjaottor, A. A., & Mensah, A. A. (2021). Spatial prediction and mapping of water quality of Owabi reservoir from satellite imageries and machine learning models. *The Egyptian Journal of Remote Sensing and Space Science*, *24*(3), 825–833. https://doi.org/10.1016/j.ejrs.2021.06.006

Aggarwal, S. (2004). *Principles of remote sensing. Satellite remote sensing and GIS applications in agricultural meteorology*.

Ahmed, M., Mumtaz, R., Anwar, Z., Shaukat, A., Arif, O., & Shafait, F. (2022). A Multi–Step Approach for Optically Active and Inactive Water Quality Parameter Estimation Using Deep Learning and Remote Sensing. *Water*, *14*(13), 2112. https://doi.org/10.3390/w14132112

Akbar, T. A., Hassan, Q. K., & Achari, G. (2014). Development of remote sensing based models for surface water quality. *CLEAN–Soil, Air, Water*, *42*(8), 1044–1051.

Al Farizi, W. S., Hidayah, I., & Rizal, M. N. (2021). Isolation Forest Based Anomaly Detection: A Systematic Literature Review. *2021 8th International Conference on Information Technology, Computer and Electrical Engineering (ICITACEE)*, 118–122. https://doi.org/10.1109/ICITACEE53184.2021.9617498

Al-Imam, A. (2019). Optimizing linear models via sinusoidal transformation for boosted machine learning in medicine. *Journal of the Faculty of Medicine Baghdad*, *61*(3, 4).

Atkinson, P. M., & Curran, P. J. (1997). Choosing an appropriate spatial resolution for remote sensing investigations. *Photogrammetric Engineering & Remote Sensing*.

Breiman, L. (2001). Random Forests. *Machine Learning*, *45*(1), 5–32. https://doi.org/10.1023/A:1010933404324

Cairo, C., Barbosa, C., Lobo, F., Novo, E., Carlos, F., Maciel, D., Flores Júnior, R., Silva, E., & Curtarelli, V. (2019). Hybrid Chlorophyll-a Algorithm for Assessing Trophic States of a Tropical Brazilian Reservoir Based on MSI/Sentinel-2 Data. *Remote Sensing*, *12*(1), 40. https://doi.org/10.3390/rs12010040

Canfield, D. E., & Hoyer, M. V. (1988). The Eutrophication of Lake Okeechobee. *Lake and Reservoir Management*, *4*(2), 91–99. https://doi.org/10.1080/07438148809354817

Chawira, M., Dube, T., & Gumindoga, W. (2013). Remote sensing based water quality monitoring in Chivero and Manyame lakes of Zimbabwe. *Physics and Chemistry of the Earth, Parts A/B/C*, *66*, 38–44. https://doi.org/10.1016/j.pce.2013.09.003

Chebud, Y., Naja, G. M., Rivero, R. G., & Melesse, A. M. (2012). Water Quality Monitoring Using Remote Sensing and an Artificial Neural Network. *Water, Air, & Soil Pollution*, *223*(8), 4875–4887. https://doi.org/10.1007/s11270-012-1243-0

Chen, J., Chen, S., Fu, R., Li, D., Jiang, H., Wang, C., Peng, Y., Jia, K., & Hicks, B. J. (2022). Remote Sensing Big Data for Water Environment Monitoring: Current Status, Challenges, and Future Prospects. *Earth's Future*, *10*(2), e2021EF002289. https://doi.org/10.1029/2021EF002289

Chen, J., De Hoogh, K., Gulliver, J., Hoffmann, B., Hertel, O., Ketzel, M., Bauwelinck, M., Van Donkelaar, A., Hvidtfeldt, U. A., Katsouyanni, K., Janssen, N. A. H., Martin, R. V., Samoli, E., Schwartz, P. E., Stafoggia, M., Bellander, T., Strak, M., Wolf, K., Vienneau, D., … Hoek, G. (2019). A comparison of linear regression, regularization, and machine learning algorithms to develop Europe-wide spatial models of fine particles and nitrogen dioxide. *Environment International*, *130*, 104934. https://doi.org/10.1016/j.envint.2019.104934

Chen, Y., Xu, P., Chu, Y., Li, W., Wu, Y., Ni, L., Bao, Y., & Wang, K. (2017). Short-term electrical load forecasting using the Support Vector Regression (SVR) model to calculate the demand response baseline for office buildings. *Applied Energy*, *195*, 659–670. https://doi.org/10.1016/j.apenergy.2017.03.034

Chicco, D., Warrens, M. J., & Jurman, G. (2021). The coefficient of determination R-squared is more informative than SMAPE, MAE, MAPE, MSE and RMSE in regression analysis evaluation. *PeerJ Computer Science*, *7*, e623. https://doi.org/10.7717/peerj-cs.623

Claverie, M., Ju, J., Masek, J. G., Dungan, J. L., Vermote, E. F., Roger, J.-C., Skakun, S. V., & Justice, C. (2018). The Harmonized Landsat and Sentinel-2 surface reflectance data set. *Remote Sensing of Environment*, *219*, 145–161. https://doi.org/10.1016/j.rse.2018.09.002

Curran-Everett, D. (2018). Explorations in statistics: The log transformation. *Advances in Physiology Education*, *42*(2), 343–347. https://doi.org/10.1152/advan.00018.2018

Dall'Olmo, G., Gitelson, A. A., Rundquist, D. C., Leavitt, B., Barrow, T., & Holz, J. C. (2005). Assessing the potential of SeaWiFS and MODIS for estimating chlorophyll concentration in turbid productive waters using red and near-infrared bands. *Remote Sensing of Environment*, *96*(2), 176–187. https://doi.org/10.1016/j.rse.2005.02.007

Dekker, A. G., Vos, R. J., & Peters, S. W. M. (2002). Analytical algorithms for lake water TSM estimation for retrospective analyses of TM and SPOT sensor data. *International Journal of Remote Sensing*, *23*(1), 15–35. https://doi.org/10.1080/01431160010006917

Drusch, M., Del Bello, U., Carlier, S., Colin, O., Fernandez, V., Gascon, F., Hoersch, B., Isola, C., Laberinti, P., Martimort, P., Meygret, A., Spoto, F., Sy, O., Marchese, F., & Bargellini, P. (2012). Sentinel-2: ESA's Optical High-Resolution Mission for GMES Operational Services. *Remote Sensing of Environment*, *120*, 25–36. https://doi.org/10.1016/j.rse.2011.11.026

El Ouali, A., El Hafyani, M., Roubil, A., Lahrach, A., Essahlaoui, A., Hamid, F. E., Muzirafuti, A., Paraforos, D. S., Lanza, S., & Randazzo, G. (2021). Modeling and Spatiotemporal Mapping of Water Quality through Remote Sensing Techniques: A Case Study of the Hassan Addakhil Dam. *Applied Sciences*, *11*(19), 9297. https://doi.org/10.3390/app11199297

ESA. (2024). *Sentinel-2 L2A*. European Space Agency. https://docs.sentinel-hub.com/api/latest/data/sentinel-2-l2a/

Faridmarandi, S., Khare, Y. P., & Naja, G. M. (2021). Long-term regional nutrient contributions and in-lake water quality trends for Lake Okeechobee. *Lake and Reservoir Management*, *37*(1), 77–94. https://doi.org/10.1080/10402381.2020.1809036

Fernández, Á., Bella, J., & Dorronsoro, J. R. (2022). Supervised outlier detection for classification and regression. *Neurocomputing*, *486*, 77–92. https://doi.org/10.1016/j.neucom.2022.02.047

Gandhi, U. (2023). Google Earth Engine for Water Resources Management. *Google Earth Engine for Water Resources Management*. https://courses.spatialthoughts.com/gee-water-resources-management.html

Garg, V., Aggarwal, S. P., & Chauhan, P. (2020). Changes in turbidity along Ganga River using Sentinel-2 satellite data during lockdown associated with COVID-19. *Geomatics, Natural Hazards and Risk*, *11*(1), 1175–1195. https://doi.org/10.1080/19475705.2020.1782482

Garreta, R., & Moncecchi, G. (2013). *Learning scikit-learn: Machine learning in python* (Vol. 2013). Packt Publishing Birmingham.

Gholizadeh, M., Melesse, A., & Reddi, L. (2016). A Comprehensive Review on Water Quality Parameters Estimation Using Remote Sensing Techniques. *Sensors*, *16*(8), 1298. https://doi.org/10.3390/s16081298

Guo, H., Huang, J. J., Chen, B., Guo, X., & Singh, V. P. (2021). A machine learning-based strategy for estimating non-optically active water quality parameters using Sentinel-2 imagery. *International Journal of Remote Sensing*, *42*(5), 1841–1866. https://doi.org/10.1080/01431161.2020.1846222

Gupta, I., Kumar, A., Singh, C., & Kumar, R. (2015). Detection and Mapping of Water Quality Variation in the Godavari River Using Water Quality Index, Clustering and GIS Techniques. *Journal of Geographic Information System*, *07*(02), 71–84. https://doi.org/10.4236/jgis.2015.72007

Ha, T. N., Lubo-Robles, D., Marfurt, K. J., & Wallet, B. C. (2021). An in-depth analysis of logarithmic data transformation and per-class normalization in machine learning: Application to unsupervised classification of a turbidite system in the Canterbury Basin, New Zealand, and supervised classification of salt in the Eugene Island minibasin, Gulf of Mexico. *Interpretation*, *9*(3), T685–T710. https://doi.org/10.1190/INT-2021-0008.1

Haifeng Wang & Dejin Hu. (2005). Comparison of SVM and LS-SVM for Regression. *2005 International Conference on Neural Networks and Brain*, *1*, 279–283. https://doi.org/10.1109/ICNNB.2005.1614615

Hajigholizadeh, M., Moncada, A., Kent, S., & Melesse, A. M. (2021). Land–Lake Linkage and Remote Sensing Application in Water Quality Monitoring in Lake Okeechobee, Florida, USA. *Land*, *10*(2), 147. https://doi.org/10.3390/land10020147

Hassan, N., & Woo, C. S. (2021). Machine Learning Application in Water Quality Using Satellite Data. *IOP Conference Series: Earth and Environmental Science*, *842*(1), 012018. https://doi.org/10.1088/1755-1315/842/1/012018

Jensen, J. R., & Lulla, K. (1987). *Introductory digital image processing: A remote sensing perspective*.

Jin, K.-R., Hamrick, J. H., & Tisdale, T. (2000). Application of Three-Dimensional Hydrodynamic Model for Lake Okeechobee. *Journal of Hydraulic Engineering*, *126*(10), 758–771. https://doi.org/10.1061/(ASCE)0733-9429(2000)126:10(758)

Katlane, R., Dupouy, C., Kilani, B. E., & Berges, J. C. (2020). Estimation of Chlorophyll and Turbidity Using Sentinel 2A and EO1 Data in Kneiss Archipelago Gulf of Gabes, Tunisia. *International Journal of Geosciences*, *11*(10), 708–728. https://doi.org/10.4236/ijg.2020.1110035

Kavzoglu, T., & Bilucan, F. (2023). Effects of auxiliary and ancillary data on LULC classification in a heterogeneous environment using optimized random forest algorithm. *Earth Science Informatics*, *16*(1), 415–435. https://doi.org/10.1007/s12145-022-00874-9

Kumar, M., Khamis, K., Stevens, R., Hannah, D. M., & Bradley, C. (2024). In-situ optical water quality monitoring sensors—Applications, challenges, and future opportunities. *Frontiers in Water*, *6*, 1380133. https://doi.org/10.3389/frwa.2024.1380133

Kutser, T. (2009). Passive optical remote sensing of cyanobacteria and other intense phytoplankton blooms in coastal and inland waters. *International Journal of Remote Sensing*, *30*(17), 4401–4425. https://doi.org/10.1080/01431160802562305

LeCun, Y., Bengio, Y., & Hinton, G. (2015). Deep learning. *Nature*, *521*(7553), 436–444. https://doi.org/10.1038/nature14539

Li, Y., & Cheng, B. (2009). *An improved k-nearest neighbor algorithm and its application to high resolution remote sensing image classification*. 1–4.

Lichtenthaler, H. K., Buschmann, C., D□ll, M., Fietz, H.-J., Bach, T., Kozel, U., Meier, D., & Rahmsdorf, U. (1981). Photosynthetic activity, chloroplast ultrastructure, and leaf characteristics of high-light and low-light plants and of sun and shade leaves. *Photosynthesis Research*, *2*(2), 115–141. https://doi.org/10.1007/BF00028752

Lillesand, T., Kiefer, R. W., & Chipman, J. (2015). *Remote sensing and image interpretation*. John Wiley & Sons.

Lim, J., & Choi, M. (2015). Assessment of water quality based on Landsat 8 operational land imager associated with human activities in Korea. *Environmental Monitoring and Assessment*, *187*(6), 384. https://doi.org/10.1007/s10661-015-4616-1

Liu, F. T., Ting, K. M., & Zhou, Z.-H. (2008). Isolation Forest. *2008 Eighth IEEE International Conference on Data Mining*, 413–422. https://doi.org/10.1109/ICDM.2008.17

Loh, W. (2011). Classification and regression trees. *WIREs Data Mining and Knowledge Discovery*, *1*(1), 14–23. https://doi.org/10.1002/widm.8

Mishra, S., & Mishra, D. R. (2012). Normalized difference chlorophyll index: A novel model for remote estimation of chlorophyll-a concentration in turbid productive waters. *Remote Sensing of Environment*, *117*, 394–406. https://doi.org/10.1016/j.rse.2011.10.016

Mitchell, T. M. (2013). *Machine learning* (Nachdr.). McGraw-Hill.

Muharemi, F., Logofătu, D., & Leon, F. (2019). Machine learning approaches for anomaly detection of water quality on a real-world data set. *Journal of Information and Telecommunication*, *3*(3), 294–307. https://doi.org/10.1080/24751839.2019.1565653

Murphy, R. R., Curriero, F. C., & Ball, W. P. (2010). Comparison of Spatial Interpolation Methods for Water Quality Evaluation in the Chesapeake Bay. *Journal of Environmental Engineering*, *136*(2), 160–171. https://doi.org/10.1061/(ASCE)EE.1943-7870.0000121

Nair, V., & Hinton, G. E. (2010). *Rectified linear units improve restricted boltzmann machines*. 807–814.

Nguyen, Q. H., Ly, H.-B., Ho, L. S., Al-Ansari, N., Le, H. V., Tran, V. Q., Prakash, I., & Pham, B. T. (2021). Influence of Data Splitting on Performance of Machine Learning Models in

Prediction of Shear Strength of Soil. *Mathematical Problems in Engineering*, *2021*, 1–15. https://doi.org/10.1155/2021/4832864

Nielsen, M. A. (2015). *Neural networks and deep learning* (Vol. 25). Determination press San Francisco, CA, USA.

Niu, C., Tan, K., Jia, X., & Wang, X. (2021). Deep learning based regression for optically inactive inland water quality parameter estimation using airborne hyperspectral imagery. *Environmental Pollution*, *286*, 117534. https://doi.org/10.1016/j.envpol.2021.117534

O'Reilly, J., & Werdell, P. (2019). Chlorophyll algorithms for ocean color sensors-OC4. *OC5 & OC6, Remote Sens*, *715*.

Ouma, Y. O., Noor, K., & Herbert, K. (2020). Modelling Reservoir Chlorophyll- *a* , TSS, and Turbidity Using Sentinel-2A MSI and Landsat-8 OLI Satellite Sensors with Empirical Multivariate Regression. *Journal of Sensors*, *2020*, 1–21. https://doi.org/10.1155/2020/8858408

Owuor, O. S., Benedict, T. J., & Kevin, O. O. (2022). *Outlier Detection Technique for Univariate Normal Datasets*.

Pahlevan, N., Smith, B., Alikas, K., Anstee, J., Barbosa, C., Binding, C., Bresciani, M., Cremella, B., Giardino, C., Gurlin, D., Fernandez, V., Jamet, C., Kangro, K., Lehmann, M. K., Loisel, H., Matsushita, B., Hà, N., Olmanson, L., Potvin, G., … Ruiz-Verdù, A. (2022). Simultaneous retrieval of selected optical water quality indicators from Landsat-8, Sentinel-2, and Sentinel-3. *Remote Sensing of Environment*, *270*, 112860. https://doi.org/10.1016/j.rse.2021.112860

Pal, M., & Mather, P. M. (2003). An assessment of the effectiveness of decision tree methods for land cover classification. *Remote Sensing of Environment*, *86*(4), 554–565. https://doi.org/10.1016/S0034-4257(03)00132-9

Peterson, K. T., Sagan, V., & Sloan, J. J. (2020). Deep learning-based water quality estimation and anomaly detection using Landsat-8/Sentinel-2 virtual constellation and cloud computing. *GIScience & Remote Sensing*, *57*(4), 510–525. https://doi.org/10.1080/15481603.2020.1738061

Phiri, D., Simwanda, M., Salekin, S., Nyirenda, V., Murayama, Y., & Ranagalage, M. (2020). Sentinel-2 Data for Land Cover/Use Mapping: A Review. *Remote Sensing*, *12*(14), 2291. https://doi.org/10.3390/rs12142291

Qian, J., Liu, H., Qian, L., Bauer, J., Xue, X., Yu, G., He, Q., Zhou, Q., Bi, Y., & Norra, S. (2022). Water quality monitoring and assessment based on cruise monitoring, remote sensing, and deep learning: A case study of Qingcaosha Reservoir. *Frontiers in Environmental Science*, *10*, 979133. https://doi.org/10.3389/fenvs.2022.979133

Ritchie, J. C., Schiebe, F., & McHenry, J. R. (1976). Remote sensing of suspended sediments in surface waters. *Photogramm. Eng. Remote Sens*, *42*, 1539–1545.

Ritchie, J. C., Zimba, P. V., & Everitt, J. H. (2003a). Remote Sensing Techniques to Assess Water Quality. *Photogrammetric Engineering & Remote Sensing*, *69*(6), 695–704. https://doi.org/10.14358/PERS.69.6.695

Ritchie, J. C., Zimba, P. V., & Everitt, J. H. (2003b). Remote Sensing Techniques to Assess Water Quality. *Photogrammetric Engineering & Remote Sensing*, *69*(6), 695–704. https://doi.org/10.14358/PERS.69.6.695

Rodríguez-López, L., Usta, D. B., Duran-Llacer, I., Alvarez, L. B., Yépez, S., Bourrel, L., Frappart, F., & Urrutia, R. (2023). Estimation of Water Quality Parameters through a Combination of Deep Learning and Remote Sensing Techniques in a Lake in Southern Chile. *Remote Sensing*, *15*(17), 4157. https://doi.org/10.3390/rs15174157

Rolnick, D., & Tegmark, M. (2017). *The power of deeper networks for expressing natural functions*. https://doi.org/10.48550/ARXIV.1705.05502

Rouse, J. W., Haas, R. H., Schell, J. A., & Deering, D. W. (1974). Monitoring vegetation systems in the Great Plains with ERTS. *NASA Spec. Publ*, *351*(1), 309.

Sagan, V., Peterson, K. T., Maimaitijiang, M., Sidike, P., Sloan, J., Greeling, B. A., Maalouf, S., & Adams, C. (2020). Monitoring inland water quality using remote sensing: Potential and limitations of spectral indices, bio-optical simulations, machine learning, and cloud computing. *Earth-Science Reviews*, *205*, 103187. https://doi.org/10.1016/j.earscirev.2020.103187

Sakuno, Y., Yajima, H., Yoshioka, Y., Sugahara, S., Abd Elbasit, M., Adam, E., & Chirima, J. (2018). Evaluation of Unified Algorithms for Remote Sensing of Chlorophyll-a and Turbidity in Lake Shinji and Lake Nakaumi of Japan and the Vaal Dam Reservoir of South Africa under Eutrophic and Ultra-Turbid Conditions. *Water*, *10*(5), 618. https://doi.org/10.3390/w10050618

Salehin, I., & Kang, D.-K. (2023). A Review on Dropout Regularization Approaches for Deep Neural Networks within the Scholarly Domain. *Electronics*, *12*(14), 3106. https://doi.org/10.3390/electronics12143106

Scholkopf, B., Kah-Kay Sung, Burges, C. J. C., Girosi, F., Niyogi, P., Poggio, T., & Vapnik, V. (1997). Comparing support vector machines with Gaussian kernels to radial basis function classifiers. *IEEE Transactions on Signal Processing*, *45*(11), 2758–2765. https://doi.org/10.1109/78.650102

Sebastiá-Frasquet, M.-T., Aguilar-Maldonado, J. A., Santamaría-Del-Ángel, E., & Estornell, J. (2019). Sentinel 2 Analysis of Turbidity Patterns in a Coastal Lagoon. *Remote Sensing*, *11*(24), 2926. https://doi.org/10.3390/rs11242926

SFWMD, S. F. W. M. D. (n.d.). *DBHydro*. https://www.sfwmd.gov/science-data/dbhydro

Solórzano, J. V., Mas, J. F., Gao, Y., & Gallardo-Cruz, J. A. (2021). Land Use Land Cover Classification with U-Net: Advantages of Combining Sentinel-1 and Sentinel-2 Imagery. *Remote Sensing*, *13*(18), 3600. https://doi.org/10.3390/rs13183600

Soomets, T., Uudeberg, K., Jakovels, D., Brauns, A., Zagars, M., & Kutser, T. (2020). Validation and Comparison of Water Quality Products in Baltic Lakes Using Sentinel-2 MSI and Sentinel-3 OLCI Data. *Sensors*, *20*(3), 742. https://doi.org/10.3390/s20030742

Stensrud, E., Foss, T., Kitchenham, B., & Myrtveit, I. (2002). An empirical validation of the relationship between the magnitude of relative error and project size. *Proceedings Eighth IEEE Symposium on Software Metrics*, 3–12. https://doi.org/10.1109/METRIC.2002.1011320

Tian, S., Guo, H., Xu, W., Zhu, X., Wang, B., Zeng, Q., Mai, Y., & Huang, J. J. (2022). Remote sensing retrieval of inland water quality parameters using Sentinel-2 and multiple machine learning algorithms. *Environmental Science and Pollution Research*, *30*(7), 18617–18630. https://doi.org/10.1007/s11356-022-23431-9

Toming, K., Kutser, T., Laas, A., Sepp, M., Paavel, B., & Nõges, T. (2016). First Experiences in Mapping Lake Water Quality Parameters with Sentinel-2 MSI Imagery. *Remote Sensing*, *8*(8), 640. https://doi.org/10.3390/rs8080640

Toming, K., Kutser, T., Uiboupin, R., Arikas, A., Vahter, K., & Paavel, B. (2017). Mapping Water Quality Parameters with Sentinel-3 Ocean and Land Colour Instrument imagery in the Baltic Sea. *Remote Sensing*, *9*(10), 1070. https://doi.org/10.3390/rs9101070

Vapnik, V. (1999). *The nature of statistical learning theory*. Springer science & business media.

Vinciková, H., Hanuš, J., & Pechar, L. (2015). Spectral reflectance is a reliable water-quality estimator for small, highly turbid wetlands. *Wetlands Ecology and Management*, *23*(5), 933–946. https://doi.org/10.1007/s11273-015-9431-5

Wager, S., Wang, S., & Liang, P. S. (2013). Dropout training as adaptive regularization. *Advances in Neural Information Processing Systems*, *26*.

Wetzel, R., & Likens, G. (2000). Limnological analyses, 3 (ed) Springer Verlag. *Nueva York*.

Yang, H., Du, Y., Zhao, H., & Chen, F. (2022). Water Quality Chl-a Inversion Based on Spatio-Temporal Fusion and Convolutional Neural Network. *Remote Sensing*, *14*(5), 1267. https://doi.org/10.3390/rs14051267

Yang, H., Kong, J., Hu, H., Du, Y., Gao, M., & Chen, F. (2022). A Review of Remote Sensing for Water Quality Retrieval: Progress and Challenges. *Remote Sensing*, *14*(8), 1770. https://doi.org/10.3390/rs14081770

Yang, W., Zhao, Y., Wang, D., Wu, H., Lin, A., & He, L. (2020). Using Principal Components Analysis and IDW Interpolation to Determine Spatial and Temporal Changes of Surface Water Quality of Xin'anjiang River in Huangshan, China. *International Journal of Environmental Research and Public Health*, *17*(8), 2942. https://doi.org/10.3390/ijerph17082942

Yigit Avdan, Z., Kaplan, G., Goncu, S., & Avdan, U. (2019). Monitoring the water quality of small water bodies using high-resolution remote sensing data. *ISPRS International Journal of Geo-Information*, *8*(12), 553.

Zhang, F., Chan, N. W., Liu, C., Wang, X., Shi, J., Kung, H.-T., Li, X., Guo, T., Wang, W., & Cao, N. (2021). Water Quality Index (WQI) as a Potential Proxy for Remote Sensing Evaluation of Water Quality in Arid Areas. *Water*, *13*(22), 3250.

Zhang, H., Xue, B., Wang, G., Zhang, X., & Zhang, Q. (2022). Deep Learning-Based Water Quality Retrieval in an Impounded Lake Using Landsat 8 Imagery: An Application in Dongping Lake. *Remote Sensing*, *14*(18), 4505. https://doi.org/10.3390/rs14184505

Zhang, J., Burke, P., Iricanin, N., Hill, S., Gray, S., & Budell, R. (2011). Long-Term Water Quality Trends in the Lake Okeechobee Watershed, Florida. *Critical Reviews in Environmental Science and Technology*, *41*(sup1), 548–575. https://doi.org/10.1080/10643389.2010.530577

Zheng, G., & DiGiacomo, P. M. (2017). Remote sensing of chlorophyll-a in coastal waters based on the light absorption coefficient of phytoplankton. *Remote Sensing of Environment*, *201*, 331–341. https://doi.org/10.1016/j.rse.2017.09.008